İsa ŞEKER

M.S. Thesis in Physics

July - 2009

DIELECTRIC PROPERTIES OF POLYMERIC NANOCOMPOSITES OF COMPLEX AND COBALT FERRITES

by

İsa ŞEKER

July 2009

DIELECTRIC PROPERTIES OF POLYMERIC NANOCOMPOSITES OF COMPLEX AND COBALT FERRITES

by

İsa ŞEKER

A thesis submitted to

the Graduate Institute of Sciences and Engineering

of

Fatih University

in partial fulfillment of the requirements for the degree of

Master of Science

in

Physics

July 2009
Istanbul, Turkey

APPROVAL PAGE

I certify that this thesis satisfies all the requirements as a thesis for the degree of Master of Science.

Prof. Dr. Mustafa KUMRU
Head of Department

This is to certify that I have read this thesis and that in my opinion it is fully adequate, in scope and quality, as a thesis for the degree of Master of Science.

Assoc. Prof. Dr. Yüksel KÖSEOĞLU
Supervisor

Examining Committee Members

Assoc. Prof. Dr. Yüksel KÖSEOĞLU ……

Assoc. Prof. Dr. Ayhan BOZKURT ……

Dr. Mehmet Burak YILMAZ …….

It is approved that this thesis has been written in compliance with the formatting rules laid down by the Graduate Institute of Sciences and Engineering.

Assoc. Prof. Dr. Nurullah ARSLAN
Director

July 2009

DIELECTRIC PROPERTIES OF POLYMERIC NANOCOMPOSITES OF COMPLEX AND COBALT FERRITES

İsa ŞEKER

M.S. Thesis – Physics
July 2009

Supervisor: Assoc. Prof. Dr. Yüksel KÖSEOĞLU

ABSTRACT

$Ni_{0.5}Zn_{0.4}Cu_{0.1}Fe_2O_4$ and $CoFe_2O_4$ doped PMMA polymeric matrixes were investigated by dielectric spectroscopy analysis at different frequency and temperature conditions. Effect of polymer, cobalt ferrite and complex ferrite doping on the dielectric properties such as the real part of dielectric constant, ε', and conductivity , σ', were acquired throughout the performed dielectric strength and activation energy analysis and the best contributing composition, in terms of the electrical peculiarity, was also optimized in the scope of the work.

A large amount of information was obtained by the temperature and frequency dependent dielectric spectroscopy study of the samples. Equivalently doped cobalt and complex ferrite demonstrated the compatible behaviors to PMMA in all measured temperature ranges according to obtained results. Contribution of cobalt ferrite on the conductivity is more dominant while complex ferrite establishes cohesively stronger structure in the constructed matrixes in all temperatures. It was also shown that higher temperatures are more promising for the samples. Such kind of polymer matrix designs can be proposed as novel ferritic-semiconductors, which can be explicitly understood from temperature dependency of the material. High quality magnetic properties of these samples were previously revealed and

these additive electrical performances of the samples can cause novel material and device inspirations, which could be of critical importance in materials science.

Keywords: ferritic semiconductor, complex ferrite, cobalt ferrite, dielectric spectroscopy, relaxation time.

POLİMERİK KOMPLEKS VE KOBALT FERRİT NANOKOMPOZİTLERİNİN DİELEKTRİK ÖZELLİKLERİ

İsa ŞEKER

Yüksek Lisans Tezi – Fizik
Temmuz 2009

Tez Yöneticisi: Doç. Dr. Yüksel KÖSEOĞLU

ÖZ

$Ni_{0.5}Zn_{0.4}Cu_{0.1}Fe_2O_4$ ve $CoFe_2O_4$ katkılı PMMA polimerik matrisleri, dielektrik spektroskopi analiziyle farklı frekans ve sıcaklık değerlerinde incelendi. Polimer, kompleks ferrit ve kobalt ferrit katkısının reel dielektrik sabiti ε' ve reel iletkenlik σ' üzerindeki etkileri, gerçekleştirilen dielektrik güç ve aktivasyon enerjisi hesaplama yöntemleriyle araştırıldı ve dielektrik hususiyetiyle en kullanışlı olabilecek kompozisyon ortaya kondu.

Sıcaklığa ve frekansa bağlı dielektrik spektroskopi, malzemeler hakkında birçok konuda bilgi sahibi olunmasına yardımcı olmuştur. Elde edilen sonuçlara göre eşit yüzdeyle karıştırılan kobalt ve kompleks ferrit, ölçüm yapılan tüm sıcaklıklarda PMMA ile uyumluluk göstermiştir. Tüm sıcaklık değerlerinde, kobalt ferrit polymer matris içinde iletkenliğe katkı sağlarken, kompleks ferrit daha çok güçlü bir tutunma etkisi oluşturmuştur. Ayrıca malzemelerin yüksek sıcaklıklarda daha kayda değer etkiler gösterdikleri gözlemlenmiştir. Açık bir şekilde, malzemelerin sıcaklığa bağımlılıkları, bu çeşit polimerik matris tasarımların yeni nesil ferritik yarıiletkenler olarak önerilebilmelerine zemin hazırlamaktadır. Sözkonusu malzemelerin yüksek nitelikli manyetik özelliklerinin incelenmesinin yanıbaşında dielektrik özelliklerinin de incelenmesi, gelecek vadeden yeni nesil elektonik cihaz tasarımlarında malzeme bilimi açısından büyük önem taşımaktadır.

Anahtar Kelimeler: ferritik yarıiletken, kompleks ferrit, kobalt ferrit, dielektrik spektroskopi, durulma zamanı.

ACKNOWLEDGEMENT

Firstly, I would like to gratitude to my supervisor Assoc. Prof. Dr. Yüksel KÖSEOĞLU for his motivation, help, stimulating and incentive suggestions during whole time of research and for writing this thesis.

I want to thank to Prof. Dr. Mustafa KUMRU for his stimulation and motivation in my thesis.

I am also grateful to Do Kyung Kim for his generosity in supplying the novel composite materials that enables us to carry out this research.

My special thanks go to Assoc. Prof. Dr. Ayhan BOZKURT for his heartfelt helps in measurement and valuable advices, motivation and collaboration in my thesis. I am grateful to Mrs. Sevim ÜNÜGÜR ÇELİK and Ms. Ayşe ASLAN for their supports.

I am also thankful to nanosicence group member Res. Assist. Murat SERTKOL for his efforts in coping with many problems.

I am grateful to the Assoc. Prof. Dr. Said Eren San for his encouragement and significant suggestions which made this work successful. I also want to thank to Res. Assist. Mustafa Okutan for his contributions during data analysis.

Finally I want to thank to my wife Aysun for her support and patience meanwhile I prepare this thesis.

TABLE OF CONTENTS

LIST OF FIGURES

LIST OF TABLES

LIST OF SYMBOLS AND ABBREVIATIONS

α : Polarizability

N : Number of atoms

P : Polarization

E : Electric field.

q : Unit electric charge

ρ : Electric charge density

D : Dielectric displacement vector

χ : Dielectric susceptibility.

ε : Relative dielectric constant

ε_0 : Permittivity of free space

C : Capacitance

τ : Relaxation time.

Φ : Pulse-response function

α : Step-response function

ω : Angular frequency

σ : Conductivity

PMMA : Polymethyl metacrylate

CHAPTER 1

1. INTRODUCTION

The concept of nanocrystalline solid was first introduced almost thirty years ago to the field of materials science. Nanocrystalline materials are generally described in between 1nm-100nm sizes today. The surface to volume ratio of interfacial atoms increases at these orders of sizes whereas they can be neglected in conventional polycrystalline materials [1].

Nanoscale properties show different characteristics than that they are at bulk sizes. As nonoscience deals with quite small dimensions, nanotechnology improves on the borderlines of Physics, Chemistry and Biology. Since it integrates these sciences, scientists find many interdisciplinary subject areas to invent new technological advances [2].

1.1 Spinel Ferrites

Spinel ferrites are metal oxides having the general formula MFe_2O_4 where M represents a type of divalent transition metal ion or a mixture of transition metal ions having valence of +2 (M: Fe, Co, Ni, Zn etc.) [3].

Ferrites with Fe^{+3} ions are the main component and their electrical and magnetic properties are influenced by their crystal structure and chemical composition [4].

Spinel structure consists of a cubic close-packet array of oxygen atoms with tetrahedral A-site and octahedral B-site. The unit cell of spinel ferrite contains 32 oxygen atoms in cubic close packing with 8 T_d (tetrahedral) and 16 O_h (octahedral) sites as shown below [5].

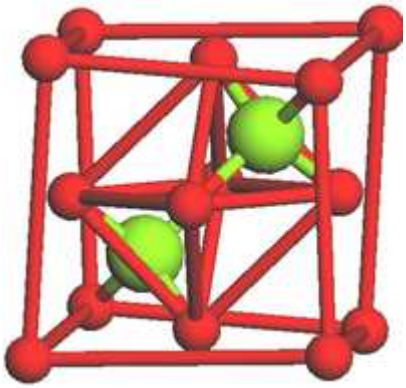

Figure 1.1 Two kinds of occupied tetrahedral sites in spinel sub-cell A. M is in green and O is in red [5].

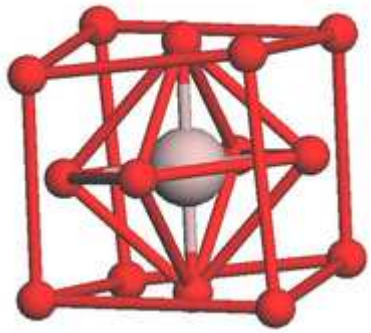

Figure 1.2 Occupied octahedral site in spinel sub-cell B. Fe is in gray, and O is in red [5].

Depending on the way that transition metal ions distribute among A and B sites, normal and inverse spinel structures are formed [6]. The distribution of cations on the octahedral and tetrahedral sites in spinel lattice being different than that they are at bulk sizes result in unusual properties. So called hopping semiconductor type mechanisms arise at these types of ferrite groups as unusual properties and the conduction processes are caused by hopping of thermally activated electrons from one cation to another [7]. Method of preparation, particle size, pH and sintering temperature can influence the distribution of these cations on the nanosized sites [8].

1.2 $CoFe_2O_4$

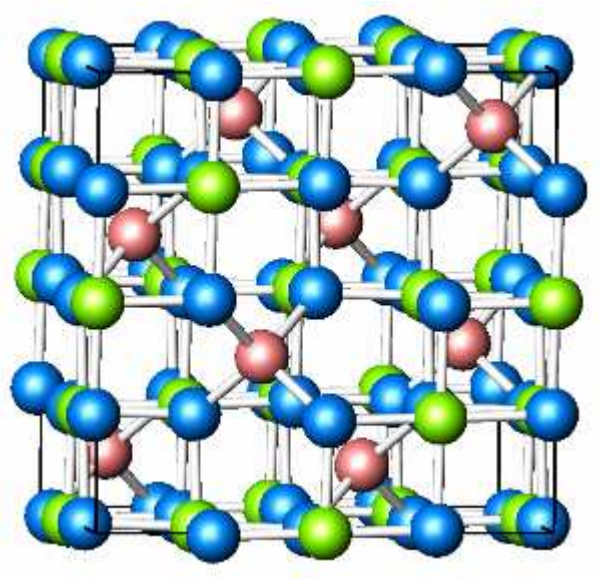

Figure 1.3 Crystal Structure of $CoFe_2O_4$ where green atoms are Co, pink atoms are Fe, and blue atoms are O [9].

Cobalt ferrite is a magnetic material with formula $CoFe_2O_4$. It is a cubic ferrite with inverse spinel structure where Co^{+2} ions are located in B sites and Fe^{+3} ions on A and B sites [10]. Due to the coupling of the spins of the cobalt and iron ions, cobalt ferrite shows strong magnetocrystalline anisotropy hence an increase in coercivity [11, 12]. High coercivity makes cobalt ferrite a good candidate for high capacity magnetic storage and magnetic anisotropy. Cobalt ferrite is a high magnetostrictive material that can be used in a wide range of applications in the automotive industry as promising stress and non-contact torque sensors [13]. Magnetostriction is the changes of shape of a magnetic material due to a magnetic field applied.

Along with its great physical and chemical stability, cobalt ferrite is preferred owing to its magnetic and electrical properties such as moderate saturation magnetization, high DC electrical resistivity and low dielectric losses [14].

1.3 Complex Ferrite ($NiZnCuFe_2O_4$)

NiZnCu ferrite is an important material that can be sintered at low temperatures and has excellent magnetic permeability. They are used as multilayer chip inductors (MLCI) and promising materials for multilayer chip LC filters [15].

NiZnCu ferrites, due to their high resistivity and permeability are used as MLCIs that operate between 300 MHz and 2 GHz. Therefore, they are used in surface mounting technology as a kind of passive component in telecommunications and portable devices [16].

1.4 Polymeric Structure

Polymethyl metacrylate (PMMA) is a kind of transparent plastic which is also sold under many trade names including plexiglas. It is preferred due to its easy handling and low cost and can be used as an alternative to glass. Polymeric matrixes can also be used in assembling composites such as different ferrite groups since they reduce the agglomeration [17]. But they are not good for wide range temperature dependent measurements as they melt at about 140 degrees. The dielectric properties of polymers are affected by the structures of the polymers. In the presence of an external electric field the dipoles are aligned with the direction of the field [18]. These materials also tend to display good insulating properties.

PMMA is a versatile material that is used in a vast range of applications in medical technologies and implants, artistic and aesthetic uses etc. The structure of PMMA is given in fig. 1.4.

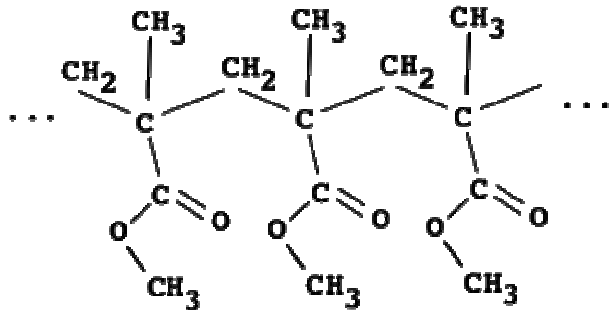

Figure 1.4 The structure of PMMA [19].

1.5 Applications of ferrites

Nanocrystalline spinel ferrites are quite useful since they promise many technological applications ranging from electronics to biology. Composite ferrite structures can be used in many areas, such as magnetic devices, switching devices, recording tapes, permanent magnets, hard disc recording media, flexible recording media, read-write heads, active components of ferrofluids, color imaging, magnetic refrigeration, detoxification of biological fluids, magnetically controlled transport of anti cancer drugs, contrast agents for magnetic resonance imaging (MRI) and magnetic cell separation and purification, etc [20-23].

Iron oxide nanobiosensors which are candidate materials for detecting odors at levels which may be imperceptible to the human nose are promising for improved food safety and quality control (toxic compounds, degradation, purity) [24].

It was revealed that $MgFe_2O_4$ and $CdFe_2O_4$ spinel ferrites are sensitive and selective to reducing gases such as LPG and C_2H_2 among some other types of ferrites tested [25]. It was also found that $NiCoMnFe_2O_4$ composition is sensitive and selective for the detection of acetone gas [26].

Among the applications, magnetic fluid hyperthermia (MFH) is a new technique for the treatment of tumor model of prostate cancer. $CoFe_2O_4$ nanoparticles are reported that they have well responded to magnetic fields at body temperature for hyperthermia cancer treatments. Magnetic nanoparticles were also used for the treatment of the ovarian cancer cells [27, 28]. Figure 1.5 shows the underlying cytoskeleton of cancer cells that had been significantly disrupted after MFH treatment.

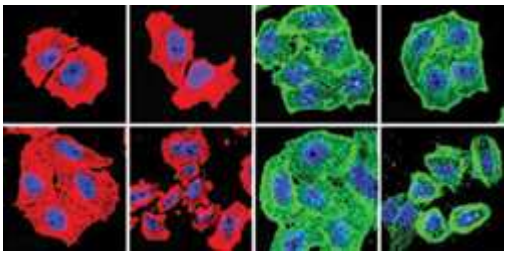

Figure 1.5 Cells exposed to nanoparticles (second row) and a magnetic field (second and fourth columns) display disrupted cytoskeletons [29].

Ferromagnetic particles are also reported to trace some pathogens and cell debris such as bacteria, dead tissue cells, and small mineral particles engulfing the solid particles namely phagocytosis [30].

In electronics, ferrites have many applications in areas such as radio, television, microwave and satellite communications and these applications are performed easily owing to low costs and easy manufacturing of these materials [4].

EM waves can be absorbed and their energies are dissipated into heat energy and this is realized by means of magnetic and dielectric losses if the characteristic impedance of free space is in perfect matching with the input characteristic impedance of the coating material [31]. It is reported that ferrites, conducting fibers, ferromagnets, and carbon nanotubes are examples of these kinds of absorbent materials [32-34]. Spinel ferrites however, work at the lower band of microwave region (1–3 GHz) because of their low natural resonance

frequencies compared with other types of ferrites [35, 36]. Appropriate choices of composition and heat treatments can enhance ferrite structure to obtain dielectric losses in wide frequency ranges [37].

Ferrites, as microwave absorbers are faciliated in order to cope with a common problem namely electromagnetic interference (EMI) and electromagnetic compatibility (EMC) in higher GHz ranges in telecommunication systems such as the mobile phones, the wireless local area network (LAN) systems, the bluetooth technologies and radars etc. [38, 39]. Microwave absorbing properties make ferrites also efficient materials for coating the exterior surfaces of high security operation aircrafts so that they can keep proceeding without being detected by radar [40]. United States (US) Air Force F-117A Nighthawk Stealth Fighter aircraft as shown in Figure 1.6 is an example of design that was made up of radar absorbent materials [41].

Figure 1.6 A US Air Force F-117A Nighthawk Stealth Fighter aircraft [41].

In this study, we have investigated the temperature dependent dielectric properties of complex and cobalt ferrite composites in a frequency range of 1Hz to 1MHz. We changed the temperature of the samples from -40^{o}C to +150^{o}C with the increments of 20^{o}C. The frequency range was swept by 43 different frequency values that cover the whole interval.

Temperature dependent dielectric spectroscopy gave us valuable information about the dielectric properties of the ferrite composites. The frequency dependent dielectric permittivity and conductivity were measured and the corresponding graphs were plotted. So, the effects of complex ferrite doping on cobalt ferrite and polymer incorporation were investigated under varying temperature and frequency values.

As a result, it was found that equally complex and cobalt ferrite doped sample has shown the best dielectric peculiarity and well compatibility with the polymeric matrix.

CHAPTER 2

2. THEORY OF DIELECTRIC SPECTROSCOPY

2.1 Historical Background

The term *dielectric* is the composition of the prefix *dia* with the word electric that refers to the passage of the electric field or flux through a material. A dielectric material does not permit electrons or in general particles to pass across it. Thus, it will not conduct electric current as being a non-conducting or insulating material. The vacuum can be regarded as the best dielectric medium, however, there may still be some remaining gas molecules even if the medium is evacuated. The so called carrier traps, due to structural defects, interact with the charge carriers and play a decisive role in dielectric mechanisms. Dielectric phenomena can be well understood by Maxwell's equations and the general electromagnetic theory [42].

In ancient times amber was rubbed to a cloth and it was seen that they attracted the tiny pieces of chaff. This attraction was a result of polarization of the charges on the amber and the small pieces. Dutch physicist Pieter van Musschenbrack is known to build the first condenser to store charges at Leyden university in 1745 but it was Faraday who first used the term capacitor at this arena almost 90 years later [43]. Figure below represents the Leyden jar condenser proposed by van Musschenbrack.

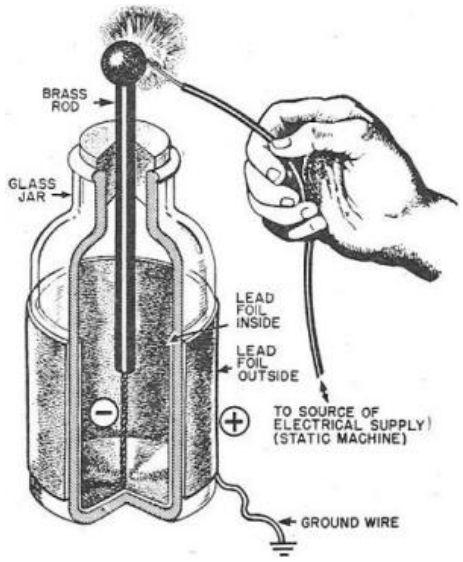

Figure 2.1 Leyden jar condenser [44].

Dielectric theories are mainly based on Maxwell's equations since they well formulate the interactions of the electromagnetic field and the material.

2.2 Classification of Dielectric Materials

Dielectric materials can be categorised as non-ferroelectric materials and ferroelectric materials. Non-ferroelectric materials, in which the electrical polarization is performed by external electric fields are grouped in three classes as nonpolar materials, polar materials and dipolar materials.

2.2.1 Non-ferroelectric Materials

Electric polarization in non-ferroelectric materials is actuated by external electric fields. Non-ferroelectric materials, depending on their polarization mechanisms can be classified into three groups: nonpolar, polar, and dipolar materials.

2.2.1.1 Non-polar Materials

Non-polar molecules have symmetric electron distribution. This results in a charge cancellation so that they have electronic polarization which is resulted from only the elastic displacement of the electron clouds by an electric field [45].

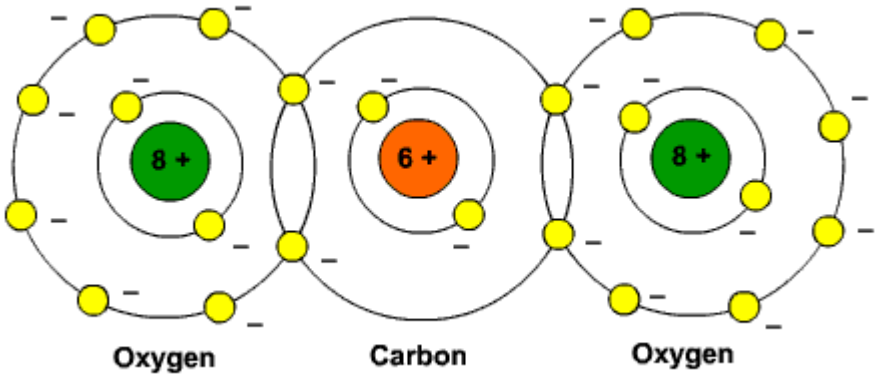

Figure 2.2 Evenly distributed electrical charges in non-polar carbon dioxide [46].

Generally, elemental materials such as silicon (Si), carbon (C) and CO_2, CH_4 and inert gases and many other materials are mentioned in this class [46]. Figure 2.2 displays the distribution of charges in CO_2.

2.2.1.2 Polar Materials

The concept of the polarity is the separation of the electric charges that leads a molecule to have an electric dipole. In polar materials, an electric field results in an elastic displacement of the valence electron clouds, changing the relative positions of the ions. As a result, such materials possess both electronic and ionic polarization [47]. Among these materials, ionic crystals, oxides, etc. can be mentioned. The total polarizability α becomes,

$$\alpha=\alpha_e+\alpha_i \tag{2.1}$$

where α_e is electronic polarizability and α_i is ionic polarizability.

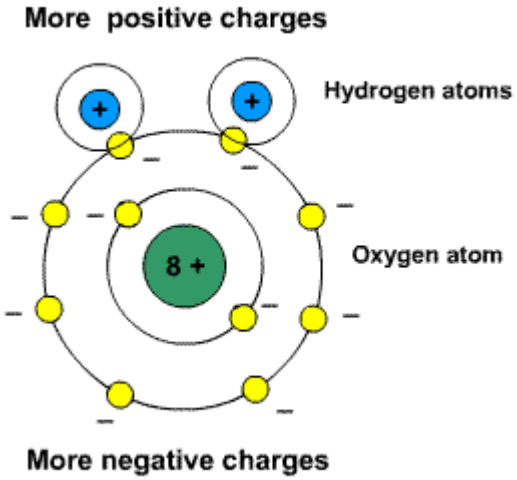

Figure 2.3 Charge distribution of a water molecule [45].

Water is a polar molecule with positive and negative charges at opposite sides. Figure 2.3 shows an example of ionic polarization in water molecule.

2.2.1.3 Dipolar Materials

Dipolar materials having all three polarization types (electronic, ionic, and orientational) possess permanent dipole moments. Therefore, their total polarizability can be expressed as:

$$\alpha=\alpha_e+\alpha_i+\alpha_o \tag{2.2}$$

where α_o is orientational polarizability.

2.2.2 Ferroelectric Materials

A ferroelectric material is the one that gains a spontaneous reversible polarization under the effect of an external electrical field. Generally, materials demonstrate ferroelectric behavior only below a certain phase transition temperature, called the Curie temperature [48]. The dielectric constant can take extremely higher values than they are in the disordered phase at Curie temperature. One can mention barium titanate ($BaTiO_3$), lead zirconate titanate ($Pb(Zr_{1-x}Ti_x)O_3$) and lithium niobate $LiNbO_3$ among the most explored ferroelectric materials with many others [49].

Ferroelectric materials show a hysteresis loop different than the ordinary dielectrics for which the polarization is a linear function of the applied electrical field. The terms ‘ferroelectricity’ and ‘ferromagnetism’ sets an anology between the electrical behaviour of these kinds of dielectrics and the magnetic behavior of some ferromagnetic compounds [48].

2.3 Dielectric Polarization

Polarization process can be defined as the ordering of the electrically charged particles under an external electric field. The capacitance of a capacitor increases with the insertion of a more polarisable material.

The stronger the applied electric field the more influence on the moments of the atoms are performed. Proportionality constant is symbolised as α. It is the measure of the ability of the material to respond to the field and also called polarizability which is also mentioned in equation 2.1. The polarization which is abbreviated as P is the electric moment per unit volume of the dielectric and expressed as:

$$P = \alpha NE \tag{2.3}$$

where N is the number of atoms, ions or molecules per unit volume and E is the applied electric field.

2.3.1 The Mechanisms of Electric Polarization

Electric polarization can be categorized under three major mechanisms: electronic polarization, ionic (sometimes called atomic) polarization and orientational polarization. At reasonable magnitudes of electric fields (electric fields much lower than the inner atomic or molecular fields), and for materials with quite low conductivity (with charge carrier effect neglected), these mechanisms dominate [50]. When an electric field is applied, it takes a certain time to reach to the stable polarization. The characteristic time depends on the type of polarization and also is different from one material to another. Hence, characteristics of a time-varying electric field has a role on the polarization response of the material.

2.3.1.1 Electronic polarization

The applied electric field shifts electron clouds and the symmetrical distribution of the of atoms or molecules no longer exist. As a result of this deformation a net electric dipole moment arises. This kind of polarization is valid for all non-conducting materials. Electronic polarization is slightly dependent on temperature since the restoring force against the displacement is relatively insensitive to temperature changes [42]. Figure 2.4 displays the shift of the positive nucleus and negatively charged electron cloud.

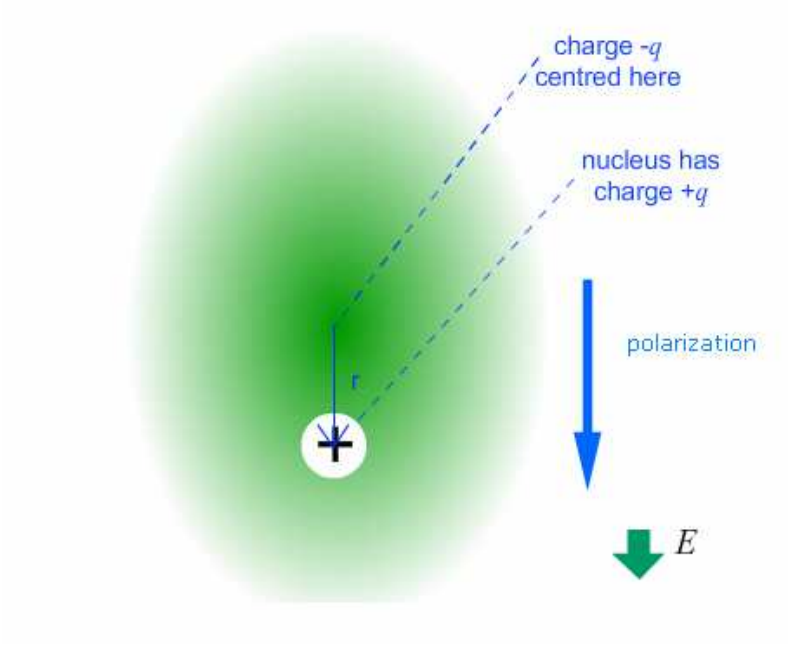

Figure 2.4 Electronic polarization under an external electric field [51].

2.3.1.2 Ionic polarization

Ionic displacement is the displacement of the negative and positive ions under the electric field. The presence of the field causes lattice vibrations as shown in figure below. This kind of polarisation is only available to materials possessing ions and permanent dipoles.

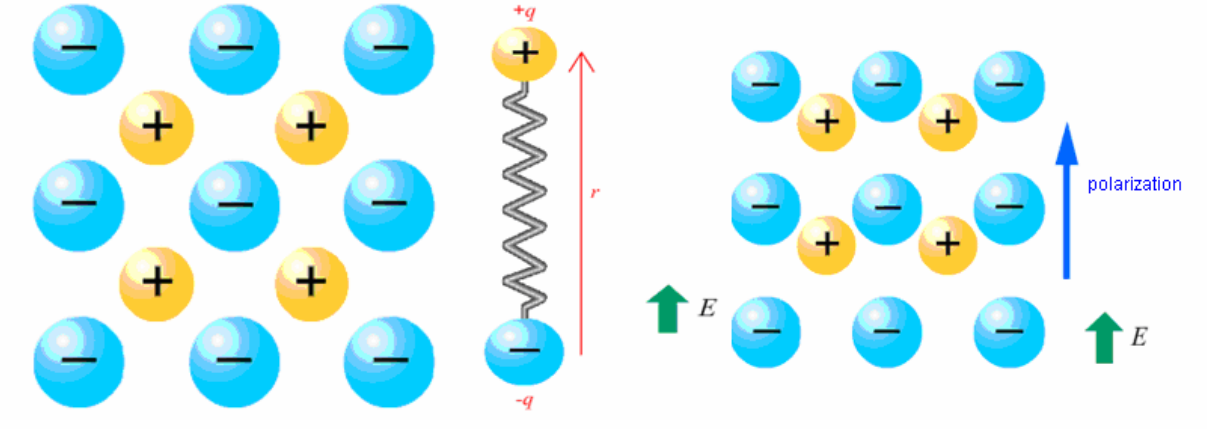

Figure 2.5 Lattice vibrations under the influence of an electric field [51].

2.3.1.3 Orientational polarization

Orientational polarization is valid for materials having molecules or particles with a permanent dipole moment [52]. In the presence of an electric, field randomly oriented dipoles are reoriented in the direction of the field as shown in the fig. 2.6. As mentioned above, elastic displacements of electron clouds and lattice vibration are in action in electronic and ionic polarization. However, movements of the dipoles in orientational polarization are like a ball rotating in a viscous liquid and they are pretty much affected by thermal agitations than other types of polarizations [51].

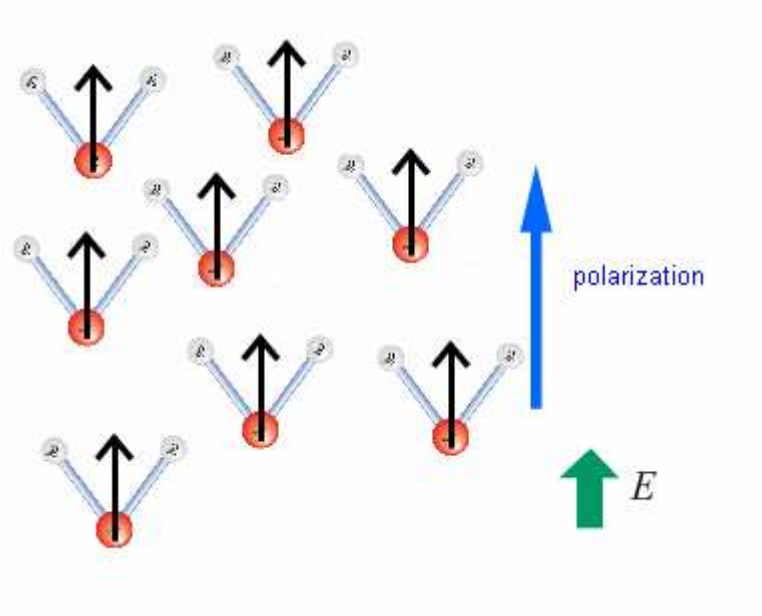

Figure 2.6 Orientation of dipoles by polarization [51].

2.4 Dielectric Constant

A steady current can not flow in dielectrics. Static electric field has non-zero value as in the case of conductors, so we derive this electric field using Maxwell's equations [53]. By averaging the exact microscopic equation of static electric field in vacuum we obtain:

$$\mathrm{curl}\boldsymbol{E} = 0 \tag{2.4}$$

and

$$\mathrm{div}\boldsymbol{E} = 4\pi\bar{\rho} \tag{2.5}$$

The total charge in the volume of a dielectric is zero, even if we place it in an electric field, therefore

$$\int \bar{\rho}\mathrm{dV} = 0 \tag{2.6}$$

Average charge density ρ can be written as follows:

$$\bar{\rho} = -\mathrm{div}\boldsymbol{P} \tag{2.7}$$

where P is the dielectric polarization.

Substituting (2.7) in (2.5) we obtain the second equation of the electrostatic field as follows:

$$\mathrm{div}\boldsymbol{D} = \boldsymbol{0} \tag{2.8}$$

where

$$\boldsymbol{D} = \boldsymbol{E} + 4\pi\boldsymbol{P} \tag{2.9}$$

D, which is the dielectric displacement vector, is also called the dielectric induction [54]. The dependence of **P** on **E** can take several forms:

$$\boldsymbol{P} = \chi\boldsymbol{E} \tag{2.10}$$

The polarization is proportional to the field strength. The proportionality factor χ is called the dielectric susceptibility.

$$\boldsymbol{D} = \boldsymbol{E} + 4\pi\boldsymbol{P} = (1 + 4\pi\chi)\boldsymbol{E} = \varepsilon\boldsymbol{E} \tag{2.11}$$

where ε is called the dielectric permittivity or the dielectric constant. In general, the dielectric constant depends on the frequency of the applied field, the temperature, and the chemical composition of the system [55,56].

Let us assume two parallel plates are placed together with oppositely signed charges as shown in fig. 2.7. In the absence of any material, ε_0, the dielectric permittivity of free space is 8.85 x 10^{-12} F/m (Figure 2.7 a). When a dielectric material is inserted in between the plates, the polarization increases. Hence, we have a more capacitive value and we define a relative dielectric constant ε which is κ times ε_0 where κ has the ratio C'/C as shown in fig. 2.7 b. Here C' is the new capacitance value of the capacitor.

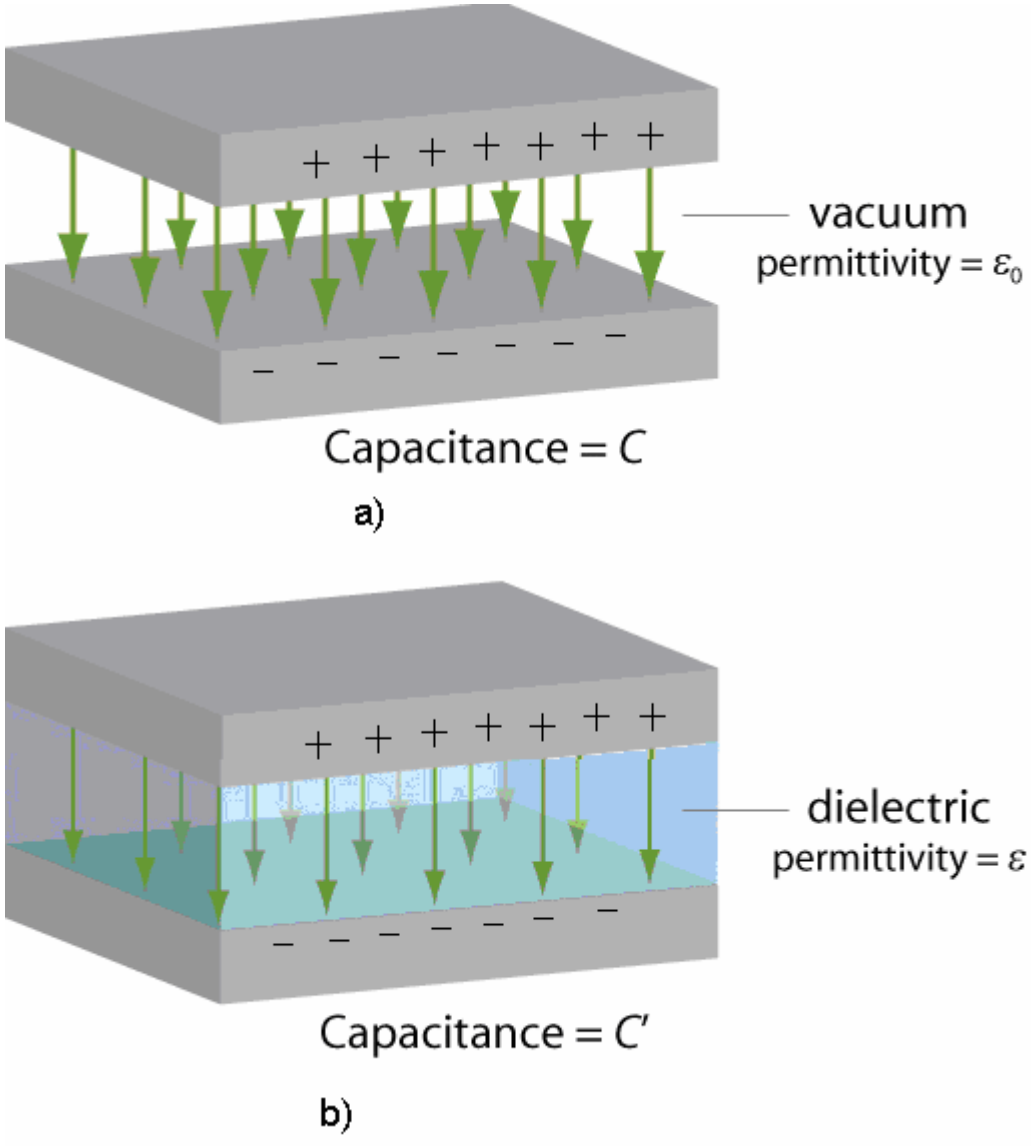

Figure 2.7 a) The permittivity of free space **b)** The relative dielectric constant [51].

2.5 The Complex Dielectric Permittivity and Conductivity

The time dependence of the dielectric displacement D for a time dependent electric field is given as follows:

$$\boldsymbol{D}(t) = \varepsilon \int_{-\infty}^{t} \boldsymbol{E}(t')\phi_D(t-t')dt' \tag{2.12}$$

If we apply the Laplace transform to the both parts and using the so called deconvolution theorem we obtain:

$$D^*(\omega) = \varepsilon^*(\omega)E^*(\omega), \tag{2.13}$$

where

$$\varepsilon^*(s) = \varepsilon_s \int_0^\infty \phi_D(t) \exp(-st) dt = \varepsilon_s L[\phi_D(t)] \tag{2.14}$$

and s=γ+iω; γ→0 and we replace s by iω [57,58].

We can rewrite (2.14) in the following way:

$$\varepsilon^*(i\omega) = \varepsilon_\infty + (\varepsilon_s - \varepsilon_\infty) L[\phi_p^{or}(t)] \tag{2.15}$$

So, the complex dielectric permittivity can be written in the following form:

$$\varepsilon^*(\omega) = \varepsilon'(\omega) - i\varepsilon''(\omega) \tag{2.16}$$

Similarly we can obtain the complex conductivity as follows:

$$\sigma^*(\omega) = \sigma'(\omega) - i\sigma''(\omega) \tag{2.17}$$

The real part of the complex dielectric function ε' is related with the energy stored where the imaginary part ε" stands for the dielectric losses. The real part of the complex conductivity σ' corresponds to energy absorption. So, it is in agreement with ε". The imaginary part of the complex conductivity σ" is related with an out of phase current that is comparable with ε' [53].

2.6 Dielectric Relaxation and Debye's Formulas

Dielectric relaxation can be defined as an instantaneous latency in the dielectric behavior of a material. This usually occurs when the polarization mechanism responses to the external electric field. If we denote the proportionality constant by 1/τ, where τ is what we call the relaxation time, we can obtain (2.18) for the orientational polarization assuming that there is no electric field:

$$\dot{\boldsymbol{P}}_{or}(t) = -\frac{1}{\tau} \boldsymbol{P}_{or}(t) \tag{2.18}$$

The solution of the above equation is:

$$\boldsymbol{P}_{or}(t) = \boldsymbol{P}_{or}(0)e^{-t/\tau} \tag{2.19}$$

The step-response function of the orientational polarization is expressed by the exponential decay:

$$\alpha_P^{or}(t) = e^{-t/\tau} \tag{2.20}$$

We can obtain an exponential decay for the pulse-response function by using (2.20)

$$\phi_p^{or} = \dot{\alpha}_P^{or}(t) = -\frac{1}{\tau}e^{-t/\tau} \tag{2.21}$$

Substituting (2.21) into (2.15) we can find the complex dielectric permittivity in the following form:

$$\varepsilon^*(\omega) = \varepsilon_\infty + (\varepsilon_s - \varepsilon_\infty)\frac{1}{\tau}L[e^{-t/\tau}] = \varepsilon_\infty + \frac{\varepsilon_s - \varepsilon_\infty}{1 + i\omega\tau} \tag{2.22}$$

seperating the real and imaginary parts of eqn. (2.22), one obtains:

$$\varepsilon'(\omega) = \varepsilon_\infty + \frac{\varepsilon_s - \varepsilon_\infty}{1 + \omega^2\tau^2} \tag{2.23}$$

and

$$\varepsilon''(\omega) = \frac{(\varepsilon_s - \varepsilon_\infty)\omega\tau}{1 + \omega^2\tau^2} \tag{2.24}$$

The equations (2.23) and (2.24) are named as the Debye's formulas. Figure. 2.8 shows the graphical way of expression of the frequency-dependence of the permittivity of a material according to Debye's formulas [53,59].

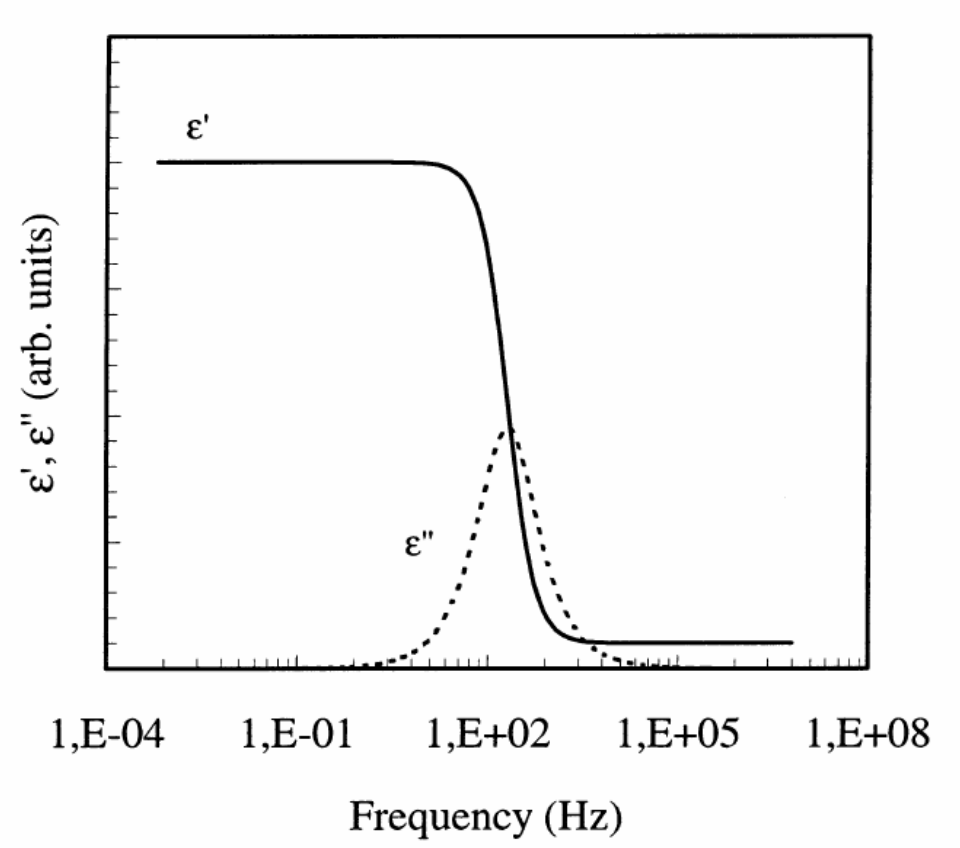

Figure 2.8 Normalized sketch of the frequency variation of the real and imaginary parts of the complex relative permittivity of a material for a relaxation time of 1 ms [59].

CHAPTER 3

3. EXPERIMENTAL

3.1 Materials

All the chemicals were of reagent grade and used without further purification if not mentioned otherwise. Methyl methacrylate (MMA) 3-aminopropyltrimethoxysilane (APTMS, $C_6H_{17}NO_3Si$), Acetic acid (C_2H_4O > 99%), Hydrochloric acid and Sodium hydroxide (NaOH) were obtained from Aldrich. 2,2'-Azobisisobutyronitrile (AIBN, $C_8H_{12}N_4$ > 98%) was obtained from Acros Organics. Pluronic® F87 NF (surfactant) was kindly gifted by BASF. Two kinds of 3- Methacryloxypropyltrimethoxysilane ($C_{10}H_{20}O_5Si$) were kindly gifted by OSi (A-174 NT) and WACKER (Silane GF31) [40].

3.2 Synthesis

The complex ferrite system is composed of Zn^{2+}, Cu^{2+}, Ni^{2+} metal ions and has the formula of $Ni_{0.5}Zn_{0.4}Cu_{0.1}Fe_2O_4$. Thermodynamic modeling (Fig. 3.1) of the complex system shows that all the species required for the formation of the system are present in the form of oxide or hydroxide at a wide pH range of 7-14. Therefore, it is possible to obtain the complex ferrite phase by using the coprecipitation in that pH range. $CoFe_2O_4$ was also synthesized based on similar modeling. Microwave absorption properties can be enhanced by increasing the crystallinity of the sample. Consequently, different heat treatments have been performed on samples of the complex ferrite system. Five samples have been prepared and each has been annealed at 700, 800, 900, 1000 and 1100 ^oC for 2 hrs. X-ray powder diffraction was used to determine the crystalline phases, and the effect of the heat treatment on the crystallinity and

the crystal growth. After the precipitation, the as-synthesized ferrite nanoparticle were silanized with APTMS [40].

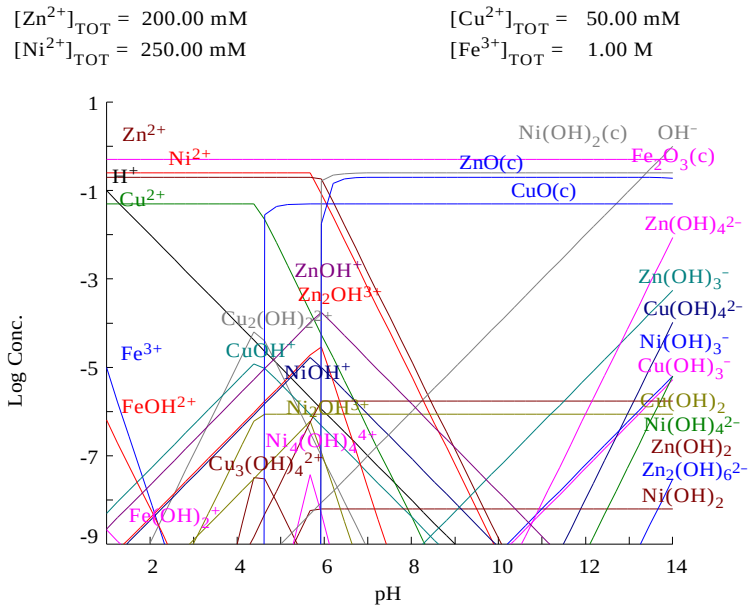

Figure 3.1 Thermodynamic modeling of Fe^{3+}-Zn^{2+}-Ni^{2+}-Cu^{2+}-H^{+}-Cl^{-} system [40].

The $Ni_{0.5}Zn_{0.4}Cu_{0.1}Fe_2O_4$ and $CoFe_2O_4$ colloidal solutions were transferred into the 3 neck flask with water cooled condenser, temperature controller and N_2 gas flowing. The silanization was performed 24 hrs at 80 °C under vigorous stirring. APTMS acts as a coupling agent, where silanization takes place on the particle surfaces bearing hydroxyl groups in the organic solvent. This results in formation of three-dimensional polysiloxane networks. The silanized $Ni_{0.5}Zn_{0.4}Cu_{0.1}Fe_2O_4$ and $CoFe_2O_4$ were cooled down to the room temperature and the supernatant was removed from the precipitation by decantation. The precipitated powder was dried in vacuum at 120 °C for 2 hrs. Composite specimens of 10, 20 and 30 pbw of 50% $Ni_{0.5}Zn_{0.4}Cu_{0.1}Fe_2O_4$ and 50% $CoFe_2O_4$ with a 5 pbw of graphite powder was dispersed in PMMA. 50 mL MMA, 0.5wt% AIBN and 200 µL acetic acid were mixed with vigorous magnetic stirring and heated to 80 °C with reflux. After 10 minutes, the hot plate was stopped and cooled down to room temperature. A viscous polymerized PMMA solution was formed. Another 25 ml MMA solution was prepared with silanized $Ni_{0.5}Zn_{0.4}Cu_{0.1}Fe_2O_4$ and $CoFe_2O_4$ mixtures by adding the Pluronic® F87 NF with 0.1 nanopowder weight ratio. After the mixture was sonicated for 10 min in water-cooled bath, the viscous pre-polymerized PMMA solution was added into the mixture of 25 mL MMA/nanopowder/surfactant and sonicated for

5 min. in water cooled bath. The mixture was transfer into clean 3-neck flask again and reheated to 80 °C with reflux. After 10 minutes, the hot plate was cooled down to the room temperature and sonicated for 10 min in water-cooled bath. The final solution was transferred into a screw capped glass container with a diameter of 20 cm and tightly closed. The container was placed in silicon oil bath and kept at 70 °C for 48 hrs. After opening the cap of the container, the temperature was raised to 95 °C for 1 hr to evaporate the unreacted monomer [40].

3.3 Characterization

Ferrite nanoparticles with the composition $Ni_{0.5}Zn_{0.4}Cu_{0.1}Fe_2O_4$ and $CoFe_2O_4$ were synthesized by the co-precipitation method and incorporated in PMMA polymeric matrix. X-ray powder diffraction (XRD), transmission electron microscopy (TEM) and dielectric spectroscopy analysis were used to determine the internal structure and properties of the samples.

3.3.1 X-ray Powder Diffraction

Regarding the peak positions in Fig. 3.2, the X-ray diffraction pattern of $Ni_{0.5}Zn_{0.4}Cu_{0.1}Fe_2O_4$ at different heat treatment temperatures correspond well to reference patterns of $Ni_{0.5}Zn_{0.4}Cu_{0.1}Fe_2O_4$ spinel ferrites. This indicates that the spinel structure of $Ni_{0.5}Zn_{0.4}Cu_{0.1}Fe_2O_4$ has been successfully produced as a single phase by the controlled chemical co-precipitation method.

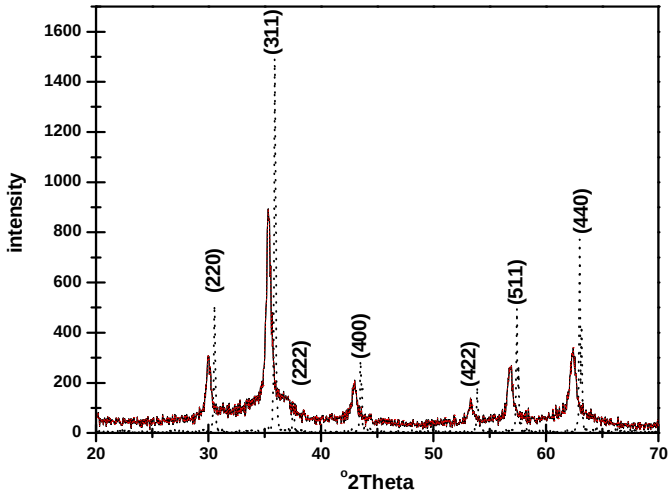

Figure 3.2 X-ray diffraction patterns of $Ni_{0.5}Zn_{0.4}Cu_{0.1}Fe_2O_4$ ferrite nanoparticles [40].

3.3.2 Transmission Electron Microscopy (TEM)

From the TEM images of $Ni_{0.5}Zn_{0.4}Cu_{0.1}Fe_2O_4$ ferrite nanoparticles shown in Fig. 3.3 a and b, as-prepared particles show rather irregular shapes comparing to the heat treated samples show spherical shapes. Moreover, the TEM image of the heat-treated samples revealed darker regions than as-prepared sample due to the crystallization [40].

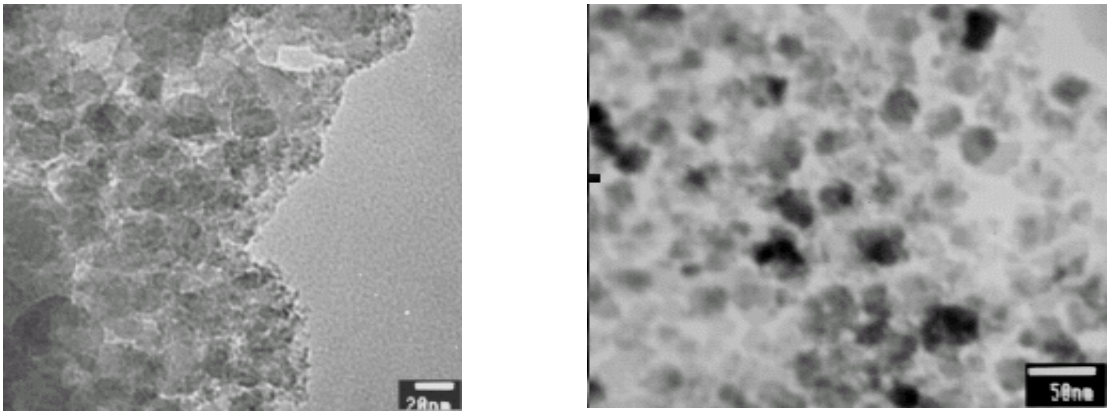

a) b)

Figure 3.3 TEM images of $Ni_{0.5}Zn_{0.4}Cu_{0.1}Fe_2O_4$ ferrite nanoparticles (a) as-prepared, (b) heat treated at 450 °C for 2 hrs [40].

3.3.3 Dielectric Measurements

Measurements were carried out in a frequency range of 1Hz-1MHz at a temperature increment of 20^{o}C from -40^{o}C to 150^{o}C under rms 1V AC. The dielectric properties of the polymeric nanocomposites containing different concentrations of ferrites have been investigated by Novocontrol Alpha-N High Resolution dielectric analyzer that is shown in fig. 3.4.

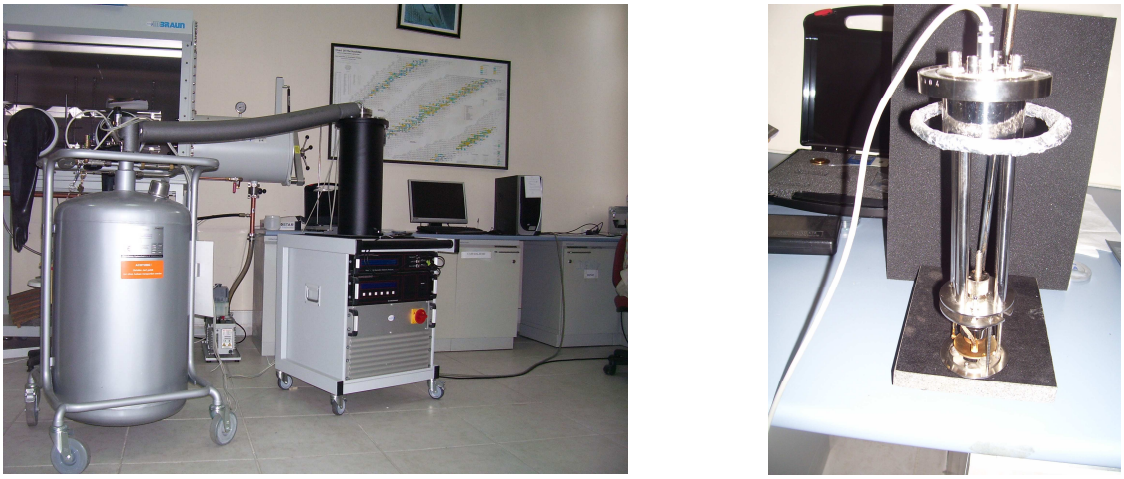

a) b)

Figure 3.4 (a) *Novocontrol* Alpha-N high resolution dielectric analyzer and (b) sample holder.

Table 4.1 shows the complex/cobalt ferrite ratios of the samples with different polymer composition. B line in Table 4.1 shows the complex ferrite/cobalt ferrite ratio of the samples. Sample A consists of totally cobalt ferrite, similarly sample E is totally complex ferrite and sample C contains 50% of each ferrite. A column represents the ferrites/PMMA ratio, so group 1 has the maximum polymer ratio where the group 3 has the minimum and the group 2 has the moderate ratio.

Table 3.1 Ferrite and polymer Composition ratios of the samples.

A:(Ferrites/PMMA) B:(complex ferrite/cobalt ferrite) ratios		**B**				
		0/100	**25/75**	**50/50**	**75/25**	**100/0**
A	**Code**	**A**	**B**	**C**	**D**	**E**
10	**1**	**1A**	**1B**	**1C**	**1D**	**1E**
20	**2**	**2A**	**2B**	**2C**	**2D**	**2E**
30	**3**	**3A**	**3B**	**3C**	**3D**	**3E**

CHAPTER 4

4. RESULTS AND DISCUSSION

We analyzed the temperature and frequency dependent dielectric spectroscopy of the samples 3A, 3B, 3C, 3D, 3E and 1C, 2C, 3C respectively in two independent groups. In this chapter, the real and the imaginary parts of complex dielectric permittivity and the real part of the conductivity were investigated.

4.1 The Real Part of the Dielectric Constant of Group 3 Samples

In this part, we analyze the ε', the real part of the dielectric constant of group 3 samples that is indicated in table 3.1.

4.1.1 The Real Part of the Dielectric Constant of Sample 3A

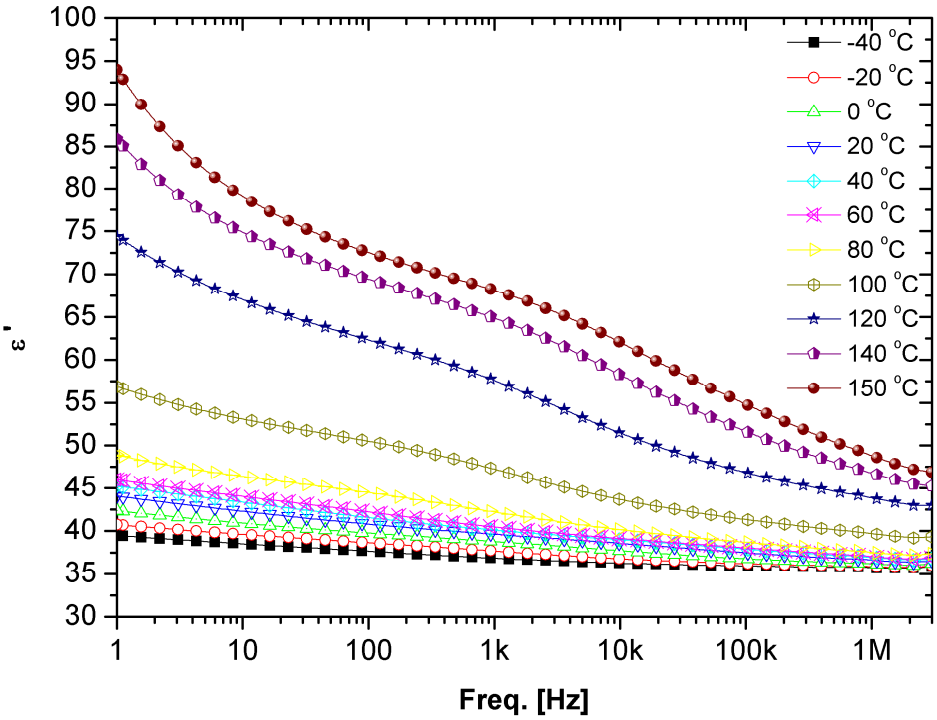

Figure 4.1 The real part of dielectric constant of the sample 3A

Figure 4.1 shows ε', the real part of dielectric constant of the sample 3A at different frequencies and temperatures. Sample 3A contains 100% cobalt ferrite, so there is no complex ferrite in this sample.

ε' values are greater at low frequencies and high temperatures. It can easily be seen that at low temperatures the permittivity values are not much affected by the increase in frequency. Therefore, we can say that is almost frequency independent at temperatures below 80^{o}C. As the temperature increases it becomes more and more frequency dependent and finally it takes its maximum value at 150^{o}C. ε' takes almost the same values varying between 40 and 45 at 1 MHz frequency range. The maximum value that is seen from the graph is 95 at 150^{o}C and 1 Hz where the minimum value is 37.5 at -40^{o}C and 1 MHz. It is distinguishable that ε' gets barely higher values at temperatures above 100^{o}C where at lower temperatures the values are squeezed and a bulge appears at moderate frequency values around 1 kHz. The reason why ε' increases with the temperature can be explained with the fact that the increase in temperature improves the segmental mobility of the polymer. So, this facilitates the polarization of polar fillers and consequently increases the dielectric constant []. The decrease

in ε' with increasing frequency can be explained by the shortening of the polarization time, hence this results in a reduction of the permittivity value as indicated by the percolation theory [60].

4.1.2 The Real Part of the Dielectric Constant of Sample 3B

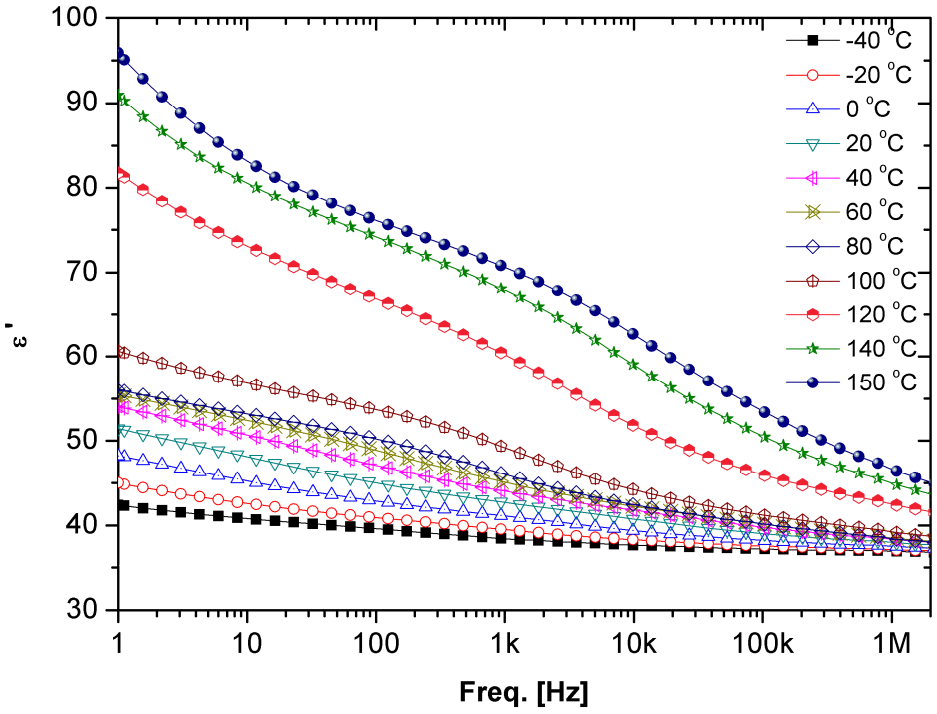

Figure 4.2 The real part of dielectric constant of the sample 3B

Figure 4.2 shows ε' values of the sample 3B at different frequencies and temperatures. Sample 3B contains 75% cobalt ferrite and 25% complex ferrite, so the affect of complex ferrite doping is starting to dominate slightly.

ε' values are again greater at low frequencies and high temperatures. It can easily be seen that at low temperatures the permittivity values are not much affected by the increase in frequency as in the case of 3A. We can say it is almost frequency independent at temperatures below 80^{o}C. As the temperature increases it becomes more and more frequency dependent and finally it takes its maximum value at 150^{o}C. ε' takes almost the same values varying between 40 and 50 at 1 MHz frequencies. The maximum value that is seen from the graph is 95 at 150^{o}C and 1 Hz where the minimum value is 40 at -40^{o}C and 1 MHz. It is noteworthy that ε' gets higher values at temperatures above 100^{o}C. It is seen that ε' gets higher values

at temperatures above 100^{o}C as in the case of 3A where at lower temperatures the values are not much squeezed.

4.1.3 The Real Part of the Dielectric Constant of Sample 3C

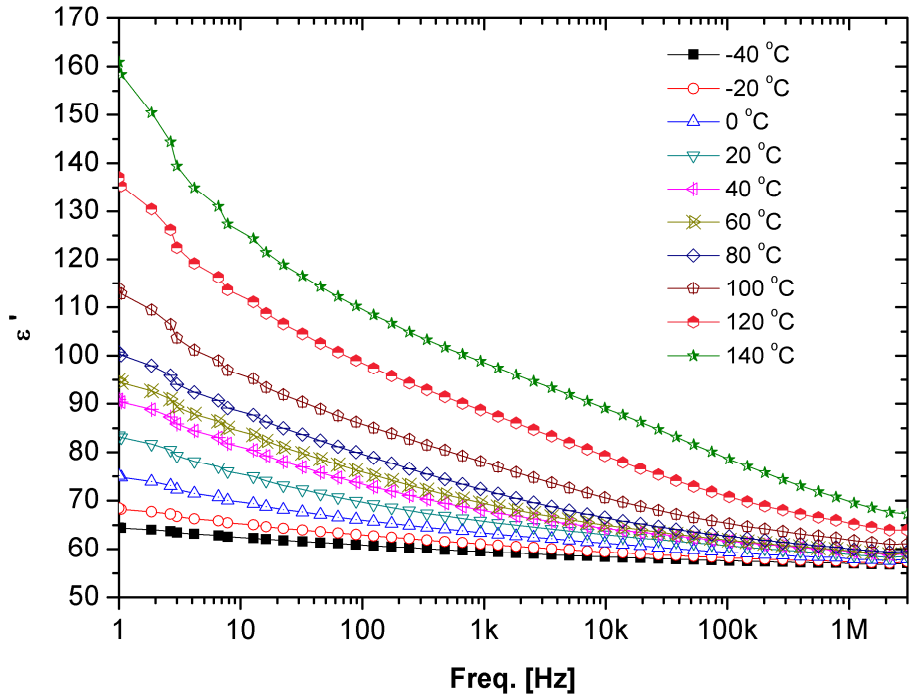

Figure 4.3 The real part of dielectric constant of the sample 3C

Figure 4.3 shows ε' values of the sample 3C at different frequencies and temperatures. Sample 3C contains 50% cobalt ferrite and 50% complex ferrite, so there is a balance in the composition ratio.

ε' values are greater at low frequencies and high temperatures as in 3A and 3B. It can again easily be seen that at low temperatures the permittivity values are not much affected by the increase in frequency. Hence, we can say values are almost frequency independent at temperatures below 0^{o}C. As the temperature increases it becomes more and more frequency dependent and finally it takes its maximum value at 140^{o}C. ε' takes almost the same values varying between 60 and 75 at 1 MHz frequency range. The maximum value that is seen from the graph is 160 at 140^{o}C and 1 Hz where the minimum value is 60 at -40^{o}C and 1 MHz. It is

noteworthy that ε' gets continuously increasing values at temperatures above 40°C different than 3A and 3B. It is also seen that ε' of 3C is much more affected by the temperature increase than in 3A and 3B and at moderate frequencies around 1 kHz does not show a convex-type appearance as 3A and 3B do.

4.1.4 The Real Part of the Dielectric Constant of Sample 3D

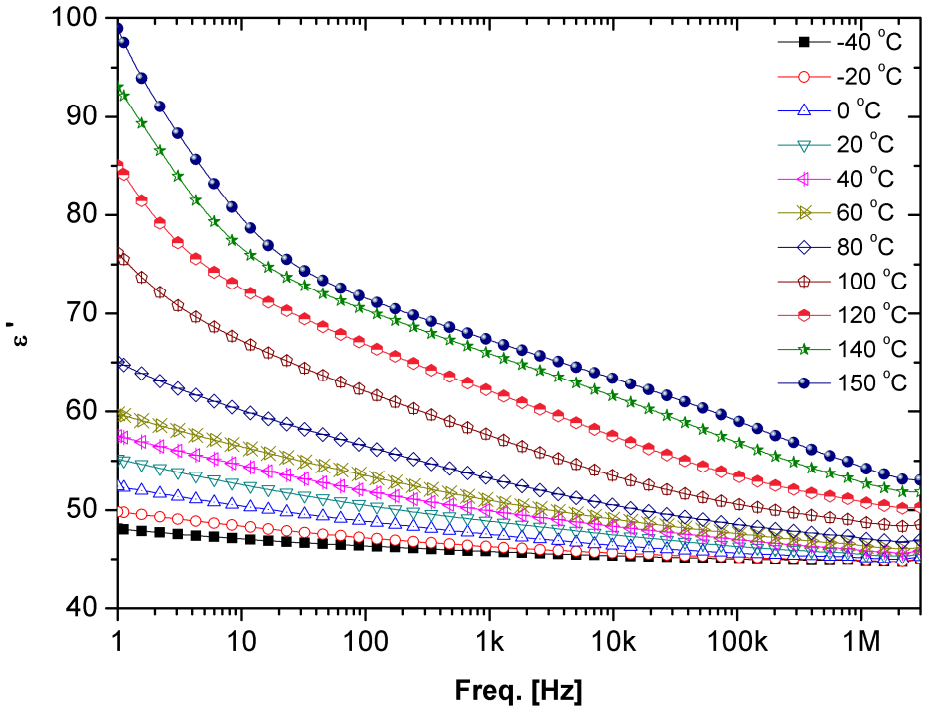

Figure 4.4 The real part of dielectric constant of the sample 3D

Figure 4.4 shows ε' values of the sample 3D at different frequencies and temperatures. Sample 3D contains 25% cobalt ferrite and 75% complex ferrite, so complex ferrite is pretty much dominant in the composition ratio.

ε' values are greater at low frequencies and high temperatures as in 3A and 3B and 3C. It is easy to verify that, at low temperatures the permittivity values are not much affected by the increase in frequency. Hence, we can see again that the values are almost frequency independent at temperatures below 0°C. As the temperature increases it becomes more and more frequency dependent and finally it takes its maximum value at 150°C. ε' takes almost the same values varying between 45 and 60 at 1 MHz frequency range. The maximum value

that is seen from the graph is 100 at 150^{o}C and 1 Hz where the minimum value is 45 at -40^{o}C and 1 MHz. It is noteworthy that ε' gets continuously increasing values at temperatures above 60^{o}C rather than 3C. It is also distinguishable that ε' values, at moderate frequencies around 1 kHz show a concave-type appearance.

4.1.5 The Real Part of the Dielectric Constant of Sample 3E

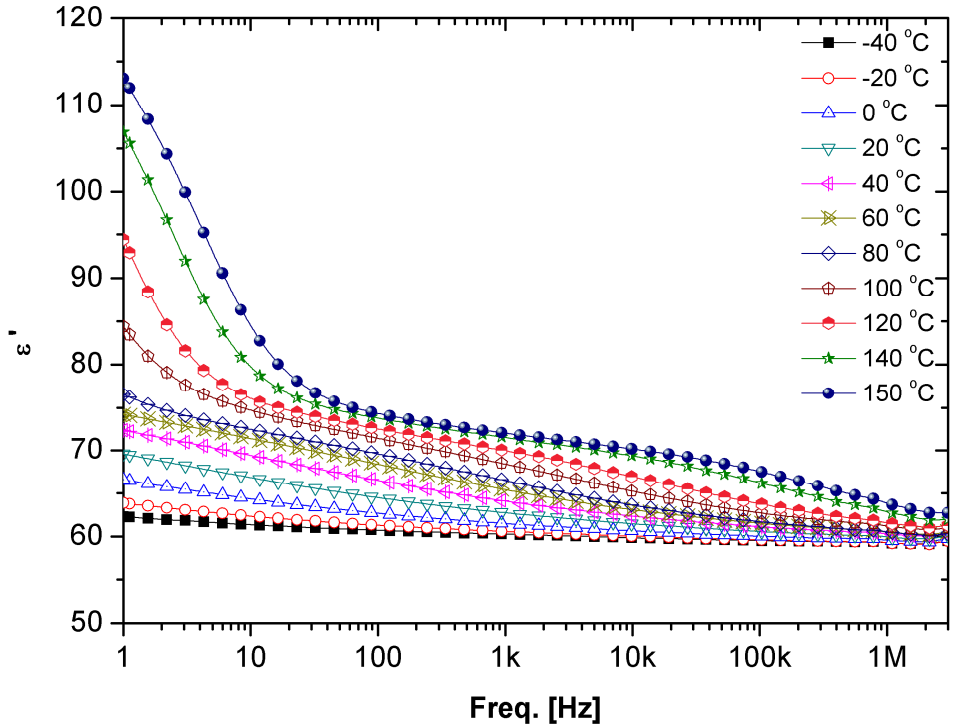

Figure 4.5 The real part of dielectric constant of the sample 3E

Figure 4.5 shows ε' values of the sample 3E at different frequencies and temperatures. Sample 3E contains 100% complex ferrite, so there is no cobalt ferrite and we see the characteristics of complex ferrite alone.

ε' values are greater at low frequencies and high temperatures as in all other samples. It is easy to verify that, at almost all temperatures except those that are greater than 100^{o}C, the permittivity values are not much affected by the increase in frequency. On the contrary, we notify that the values are strongly frequency dependent at temperatures above 100^{o}C at low frequency range. ε' takes almost the same values varying between 60 and 65 at 1 MHz

frequency range. The maximum value that is seen from the graph is 115 at 150°C and 1 Hz where the minimum value is 60 at -40°C and 1 MHz. It is noteworthy that ε' values gets quite squeezed form at moderate and high frequency range in all temperatures.

4.2 The Imaginary Part of the Dielectric Constant of Group 3 Samples

In this part, we analyze the ε'', the imaginary part of the dielectric constant of group 3 samples that is indicated in table 3.1.

4.2.1 The Imaginary Part of the Dielectric Constant of Sample 3A

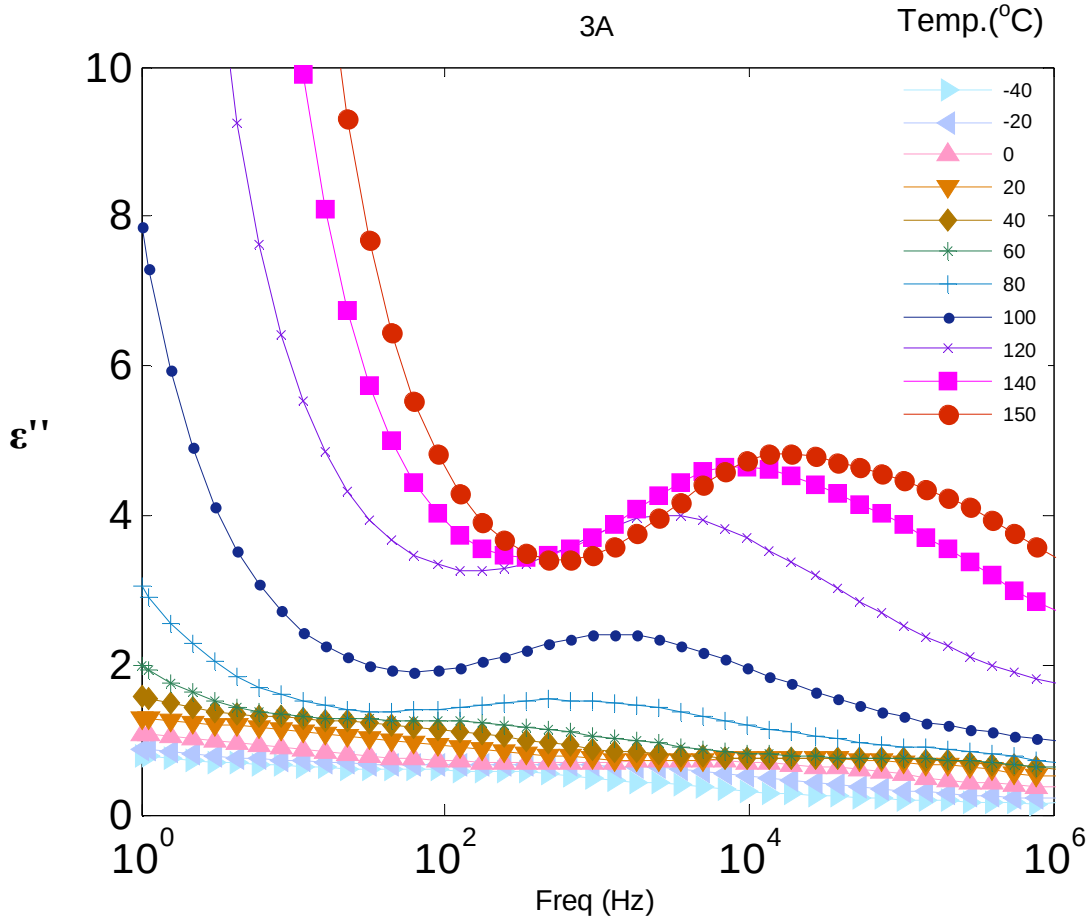

Figure 4.6 The imaginary part of dielectric constant of the sample 3A

Figure 4.6 shows ε'', the imaginary part of complex dielectric constant values of the sample 3A at different frequencies and temperatures.

First of all, ε" of the sample is strongly dependent on the temperature and frequency above 60°C whereas it has almost constant values varying between 0 and 2 at lower temperatures. At high temperatures we can mention about two distinct regions: the low frequency region and the high frequency region. We note that ε" is extremely large at low frequency and high temperature region whereas it has quite low values at high frequency regions for low temperatures. It is noticeable that 120°C is a critical temperature between the low and high ε" values. This temperature value could result in such an effect since it is the glass transition temperature, T_g of the PMMA, and its combination with the cobalt ferrite would lead to such a result. We also notice that the peak values of the high temperature values are shifted to higher frequencies as the temperature increases and one can say that these peaks correspond to dielectric relaxations. The relaxation of the polymer is the result of the cooperative rearrangement of the polymer molecular segments [61].

4.2.2 The Imaginary Part of the Dielectric Constant of Sample 3B

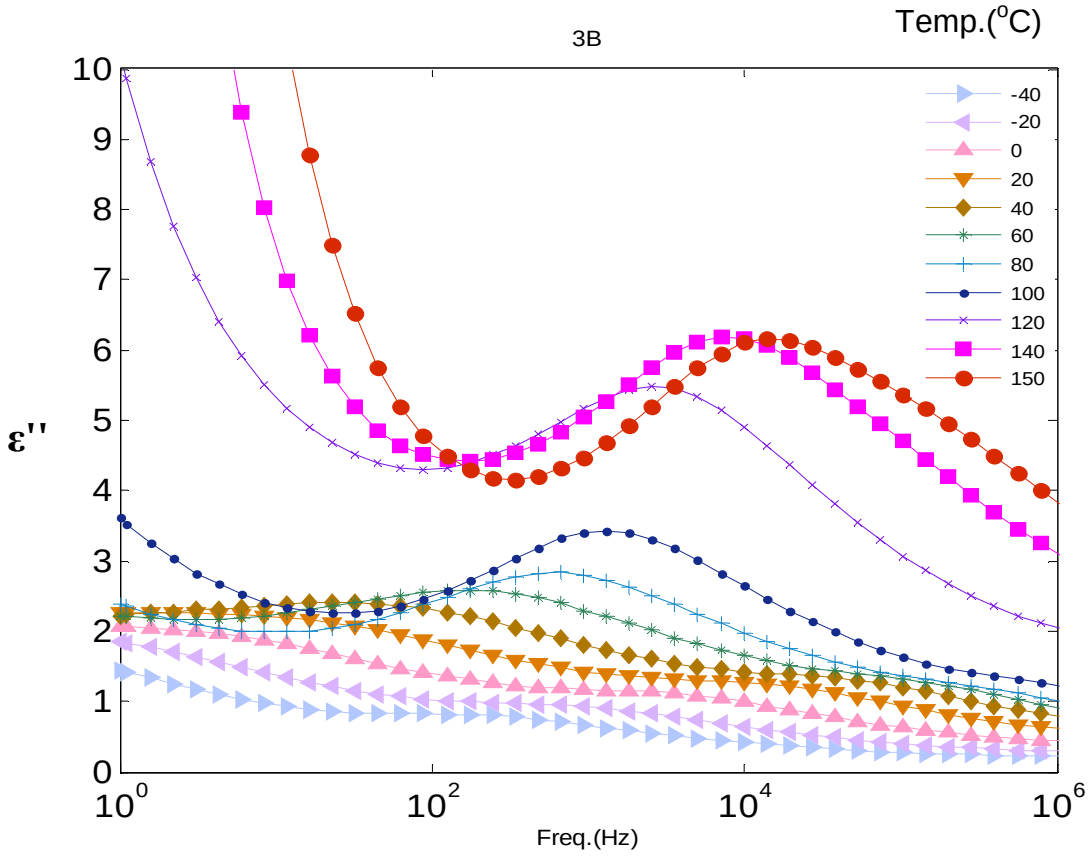

Figure 4.7 The imaginary part of dielectric constant of the sample 3B

Figure 4.7 shows ε", the imaginary part of complex dielectric constant values of the sample 3B at different frequencies and temperatures.

We see that ε" of the sample is strongly dependent on the temperature and frequency above 60°C whereas it has almost constant values varying between 0 and 2 at temperatures lower than 60°C. At high temperatures we can mention about two distinct regions again: the low frequency region and the high frequency region. We note that ε" is extremely large at low frequency and high temperature region where it has quite low values at high frequency regions for low temperatures. Here, 120°C is again a critical temperature between the low values and the high ones despite the addition of complex ferrite. This effect can also be interpreted as a consequence of the glass transition temperature of the PMMA. We also notice that the peak values of the high temperature values are also shifted to higher frequencies as in 3A.

4.2.3 The Imaginary Part of the Dielectric Constant of Sample 3C

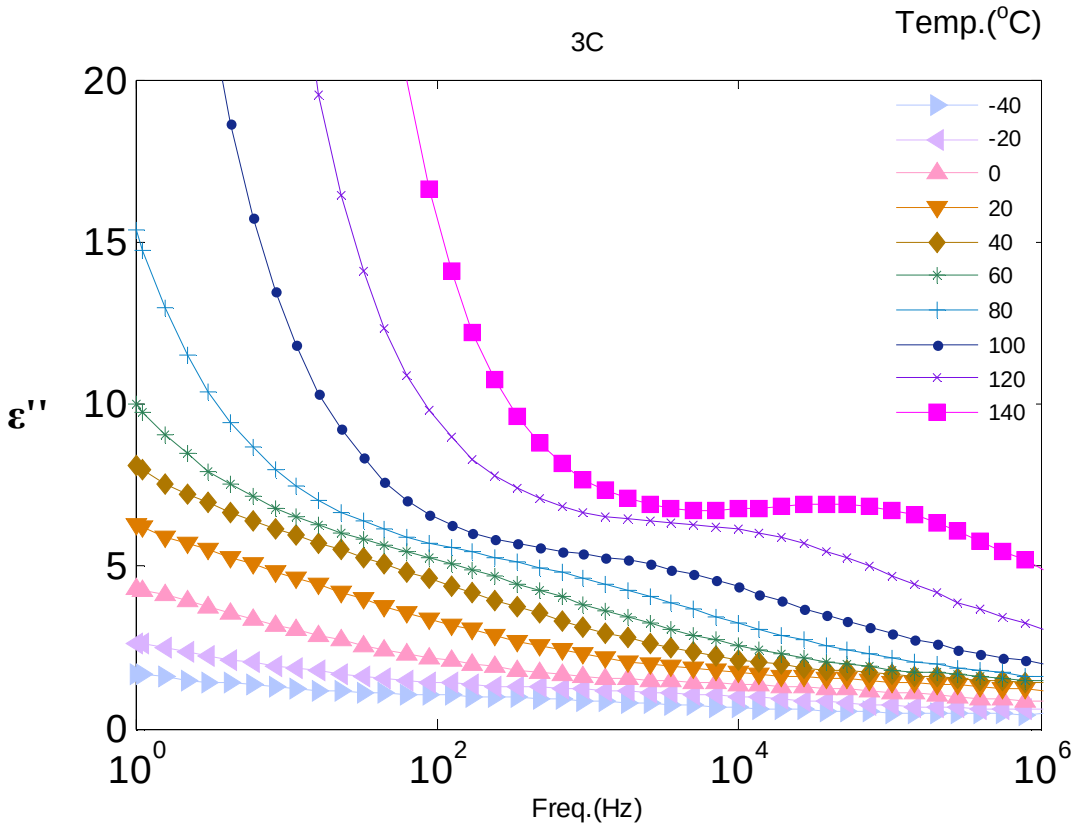

Figure 4.8 The imaginary part of dielectric constant of the sample 3C

Figure 4.8 shows ε", the imaginary part of complex dielectric constant values of the sample 3C at different frequencies and temperatures.

It is easy to see that ε" of the sample is also strongly dependent on the temperature and frequency above 60°C whereas it has almost constant values varying between 0 and 2 at temperatures lower than 60°C. At higher temperatures, there are again two distinct regions: the low frequency region and the high frequency region. We note that ε" is extremely large at low frequency and high temperature region whereas it has quite low values at high frequency regions for low temperatures. It is obvious that 3C has the highest ε" values amongst the other samples and there is no such discontinuity between the top 3 temperatures and the lower ones. Therefore we can mention the overwhelming effect of the complex ferrite on the polymeric structure and the cobalt ferrite. Consequently, we note that the peak values of the high temperature values are weakened and the relaxation phenomenon becomes less noticeable different than 3A and 3B.

4.2.4 The Imaginary Part of the Dielectric Constant of Sample 3D

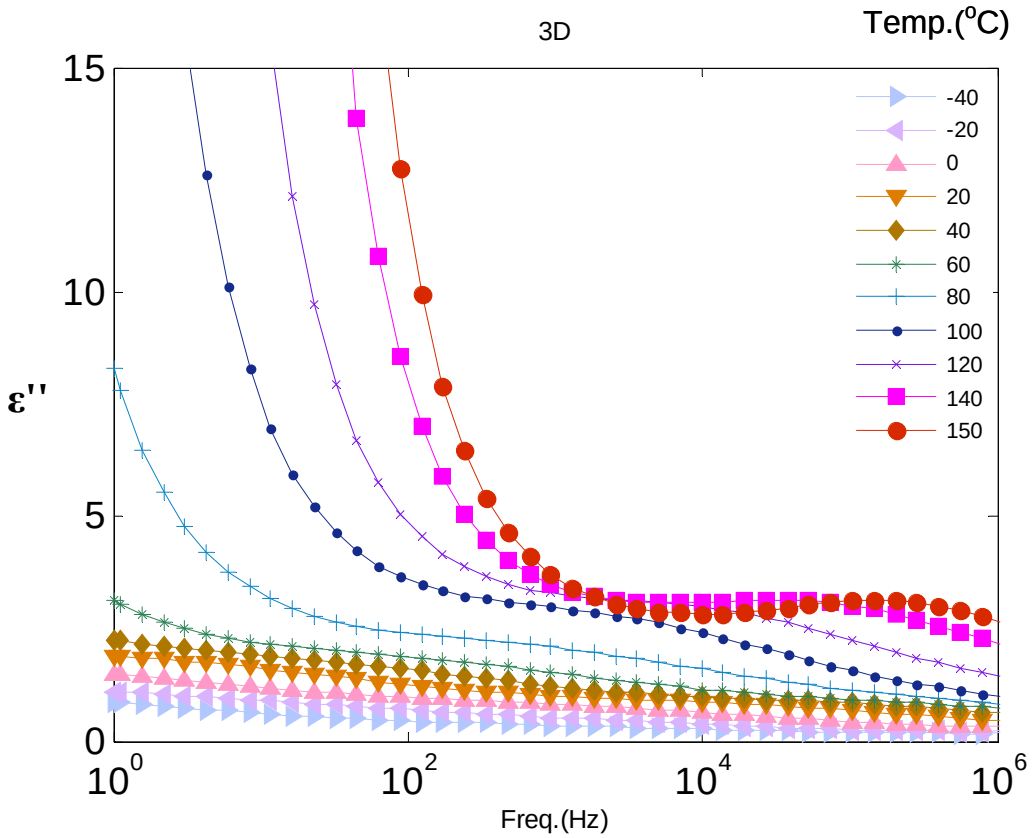

Figure 4.9 The imaginary part of dielectric constant of the sample 3D

Figure 4.9 shows ε", the imaginary part of complex dielectric constant values of the sample 3D at different frequencies and temperatures.

It is easy to see that ε" of the sample 3D is quite similar to 3C in many ways. We can again see the strong temperature and frequency dependency above 60°C whereas it has almost constant values varying between 0 and 2 at temperatures lower than 60°C. At higher temperatures, there are two distinct regions again: the low frequency region and the high frequency region. We note that ε" is extremely large at low frequency and high temperature region where it has quite low values at high frequency regions for all low temperatures. It is obvious that 3D has smaller ε" values than 3C and there is no discontinuity between the top 3 temperatures and the lower ones. It is noteworthy that 150°C value gets smaller values than 140°C value at a certain frequency range around 10 kHz. It can also be seen that the relaxation peaks of the high temperature values are weakened as in 3C.

4.2.5 The Imaginary Part of the Dielectric Constant of Sample 3E

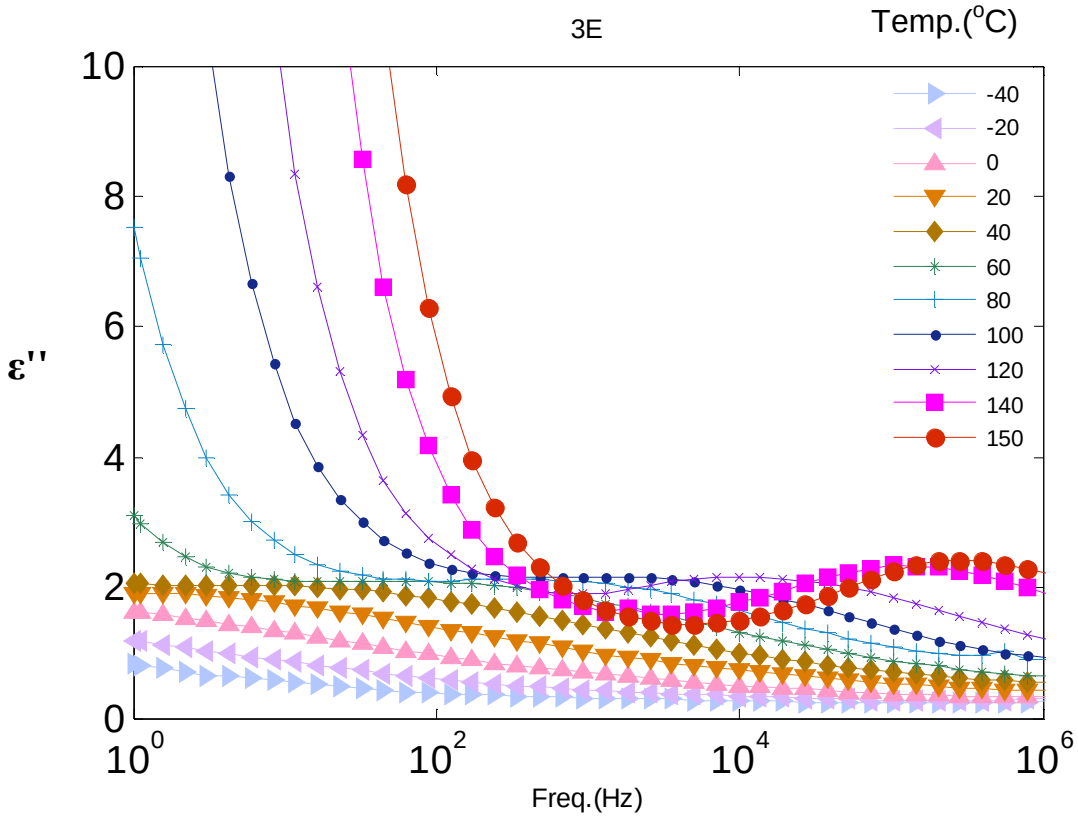

Figure 4.10 The imaginary part of dielectric constant of the sample 3E

Figure 4.10 shows ε", the imaginary part of complex dielectric constant values of the sample 3E at different frequencies and temperatures.

We can easy notify that ε" of the sample 3E is quite similar to 3C and 3D in many ways. Strong temperature and frequency dependency above 60^{o}C can be seen whereas we observe it has almost constant values varying between 0 and 2 at temperatures lower than 60^{o}C. We note that ε" is extremely large at low frequency and high temperature region where it has quite low values at high frequency regions for all low temperatures as in the case of the all samples. It is obvious that 3D has smaller ε" values than 3C and there is not a discontinuity between the top 3 temperatures and the lower ones. It is noteworthy that 150^{o}C value gets smaller values than even 80^{o}C value at a certain frequency range around 10 kHz. We can also note that the peak values of the high temperature values are become noticeable again revealing the relaxation phenomenon that is occurring as in the case of 3A and 3B.

4.3 The Real Part of the Conductivity of Group 3 Samples

In this part, we analyze the σ', the real part of the conductivity of group 3 samples that is indicated in table 3.1. Conductivity is a measure of the ability of a material to conduct electric current. It is the reciprocal of electrical resistivity and expressed as siemens per meter ($S \cdot m^{-1}$) in SI units.

4.3.1 The Real Part of the Conductivity of Sample 3A

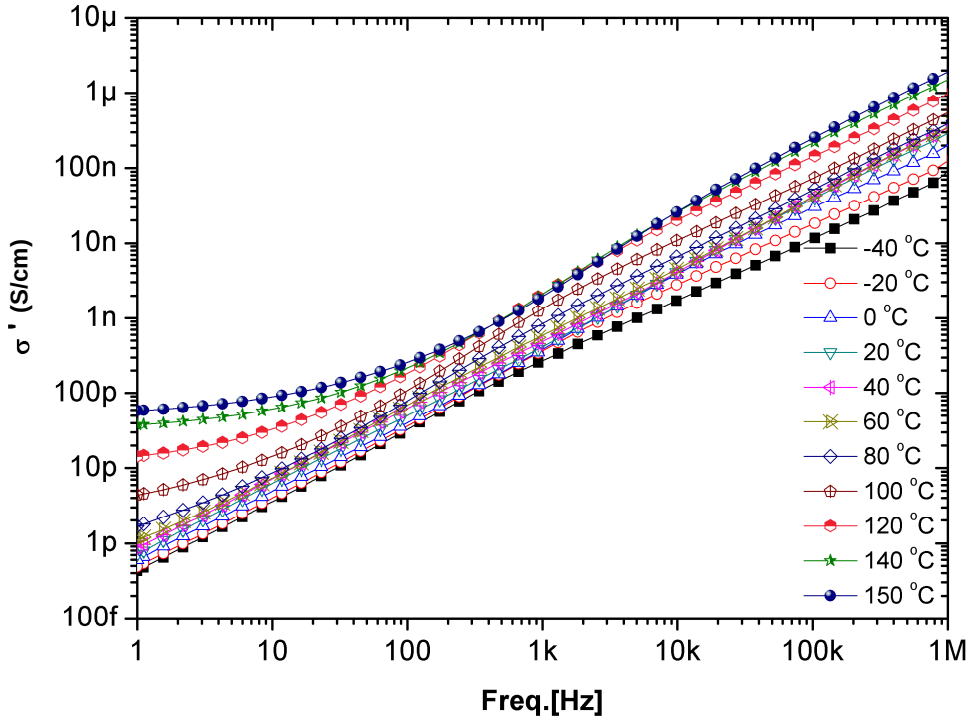

Figure 4.11 The real part of the conductivity value of the sample 3A

Figure 4.11 shows σ', the real part of the conductivity value of the sample 3A at varying temperatures and frequencies.

First of all, we can immediately see that there is a direct proportionality between the σ' value of the sample and the frequency of the external electric field applied. This is a result of the direct percolation of the ferrites with each other [62]. The conductivity values are between 10^{-12} and 10^{-6}, which is typical for ferrite oxides. So, one can see that the effect of the increasing frequency is extremely predominant on the conductivity values. Besides, we can mention the reducing affect of the polymer doping on conductivity. Moreover, the linearity of the graph is distorted after a certain temperature value like 60^{o}C. For temperatures higher than this value, we observe the distinction of the low frequency and high frequency regions. At low frequency region, we see the slight frequency dependency whereas at high frequency region the linear relationship is still conserved. These two distinct conductivity zones are interpreted as the direct current (DC) conductivity and the alternating current (AC) conductivity.

The order of the conductivity increases at about the order of 2 for 1 Hz spot frequency where the increment is at the order of 1 at the larger frequencies between the lowest and the highest temperatures.

4.3.2 The Real Part of the Conductivity of Sample 3B

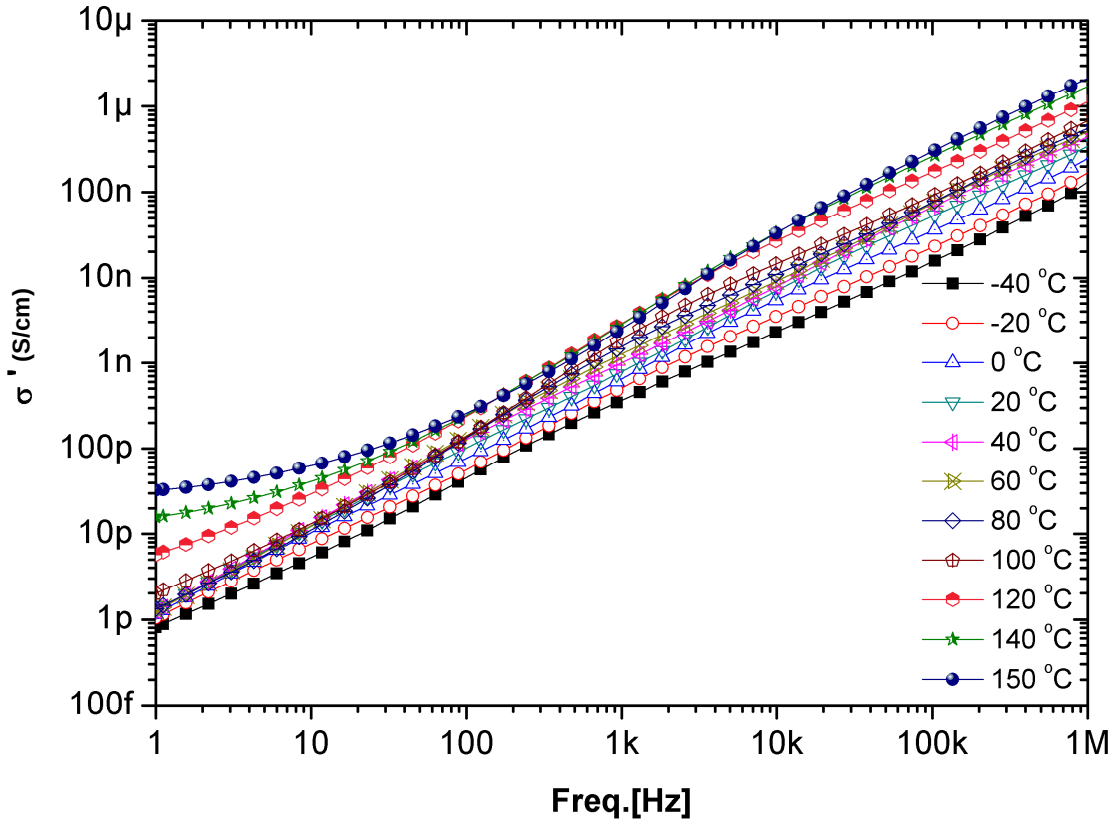

Figure 4.12 The real part of the conductivity of the sample 3B

Figure 4.12 shows σ', the real part of the conductivity value of the sample 3B at varying temperature and frequencies.

We note that that there is a direct proportionality between the σ' value of the sample and the frequency of the external electric field applied. The conductivity values are between 10^{-12} and 10^{-6} S/cm. So, we again see that the effect of the increasing frequency is extremely predominant on the conductivity values. Besides, we can mention the reducing affect of the polymer doping on the conductivity. Moreover, the linearity of the graph is distorted after a certain temperature value like 100^{o}C. For temperatures higher than this value, we observe the distinction of the low frequency and high frequency regions. At low frequency region, we see the slight frequency dependence whereas at high frequency region the linear relationship is still conserved. It is easy to see that 3B graph is quite similar to 3A except that, in 3B, the DC conductivity part is more squeezed than 3A.

4.3.3 The Real Part of the Conductivity of Sample 3C

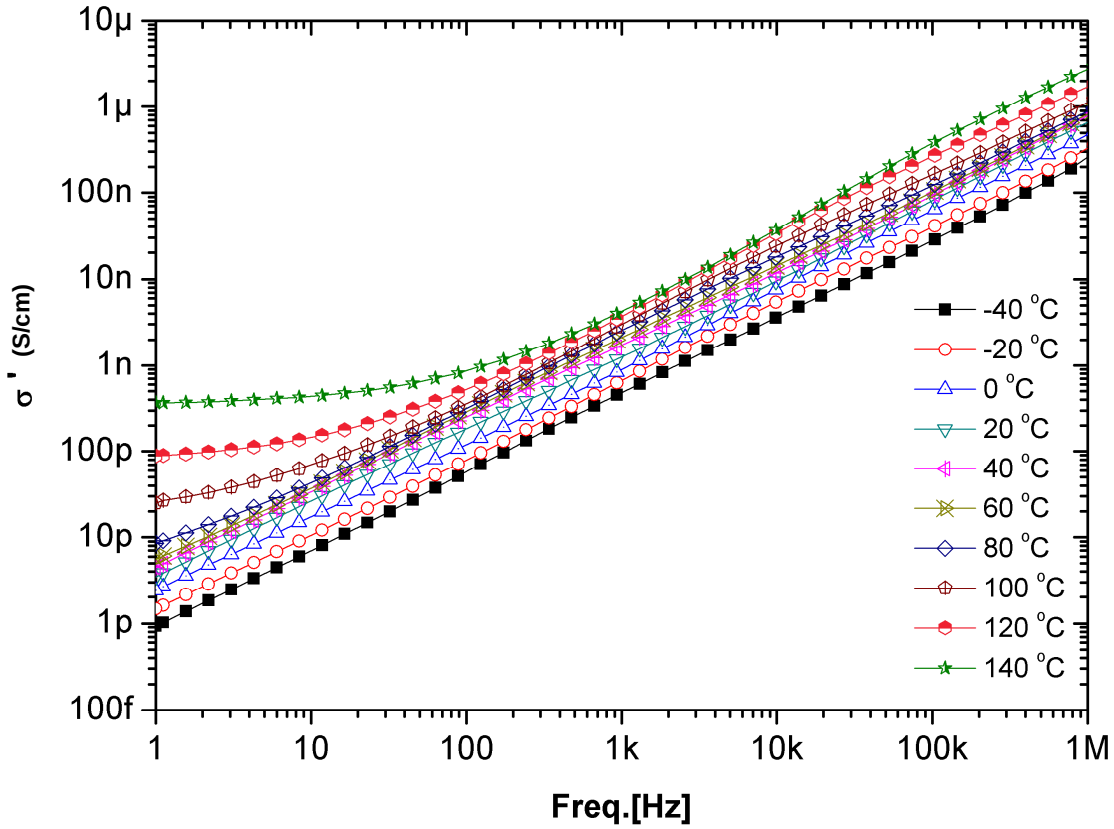

Figure 4.13 The real part of the conductivity of the sample 3C

Figure 4.13 shows σ', the real part of the conductivity value of the sample 3C at varying temperature and frequencies.

It is obvious that there is a direct proportionality between the σ' value of the sample and the frequency of the external electric field applied. The conductivity values are between 10^{-12} and 10^{-6} S/cm. Hence, one can see that the effect of the increasing frequency is extremely predominant on the conductivity values. Moreover, the linearity of the graph is distorted after a certain temperature value like 80°C. For temperatures higher than this value, we observe the distinction of the low frequency and high frequency regions. At low frequency region, we see the slight frequency dependency whereas at high frequency region the linear relationship is still conserved. The order of the conductivity almost increases at about the order of 3 for 1 Hz spot frequency where the increment is of the order of 1 at the larger frequencies between the lowest and the highest temperature. One can note that 3C graph is quite different than 3A and 3B since the DC conductivity part is more separated and the moderate frequency part is not much squeezed.

4.3.4 The Real Part of the Conductivity of Sample 3D

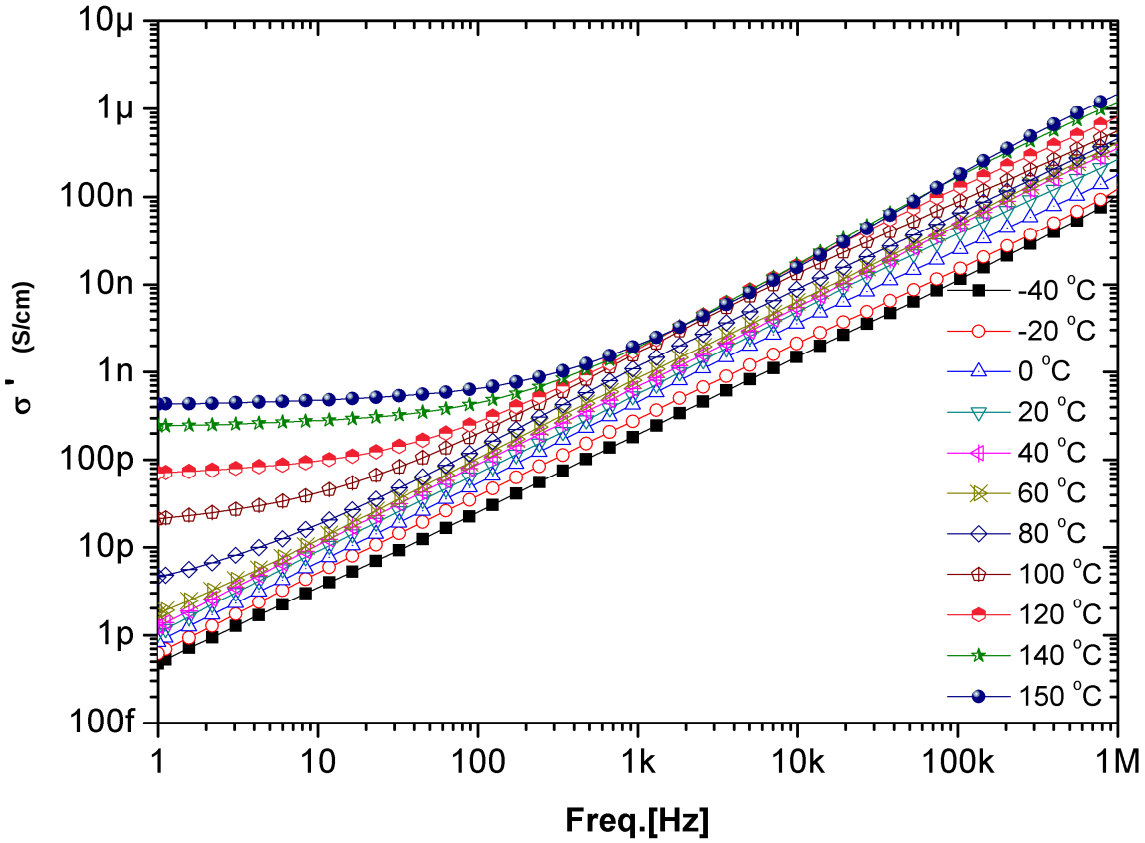

Figure 4.14 The real part of the conductivity of the sample 3D

Figure 4.14 shows σ', the real part of the conductivity value of the sample 3D at varying temperature and frequencies.

It is obvious that there is a direct proportionality between the σ' value of the sample and the frequency of the external electric field applied. The conductivity values are between 5.10^{-13} and 10^{-6} S/cm. So, we again see that the effect of the increasing frequency is extremely predominant on the conductivity values. Moreover, the linearity of the graph is distorted after a certain temperature value like 60^{o}C. For temperatures higher than this value, we observe the distinction of the low frequency and high frequency regions. At low frequency region, we see the slight frequency dependency whereas at high frequency region the linear relationship is still conserved. The order of the conductivity almost increases at about the order of 3 for 1 Hz spot frequency where the increment is larger than the order of 1 at the larger frequencies between the lowest and the highest temperature. It is easy to see that 3D graph is quite similar to 3C since the DC conductivity part is more separated and the moderate frequency part is not much squeezed.

4.3.5 The Real Part of the Conductivity of Sample 3E

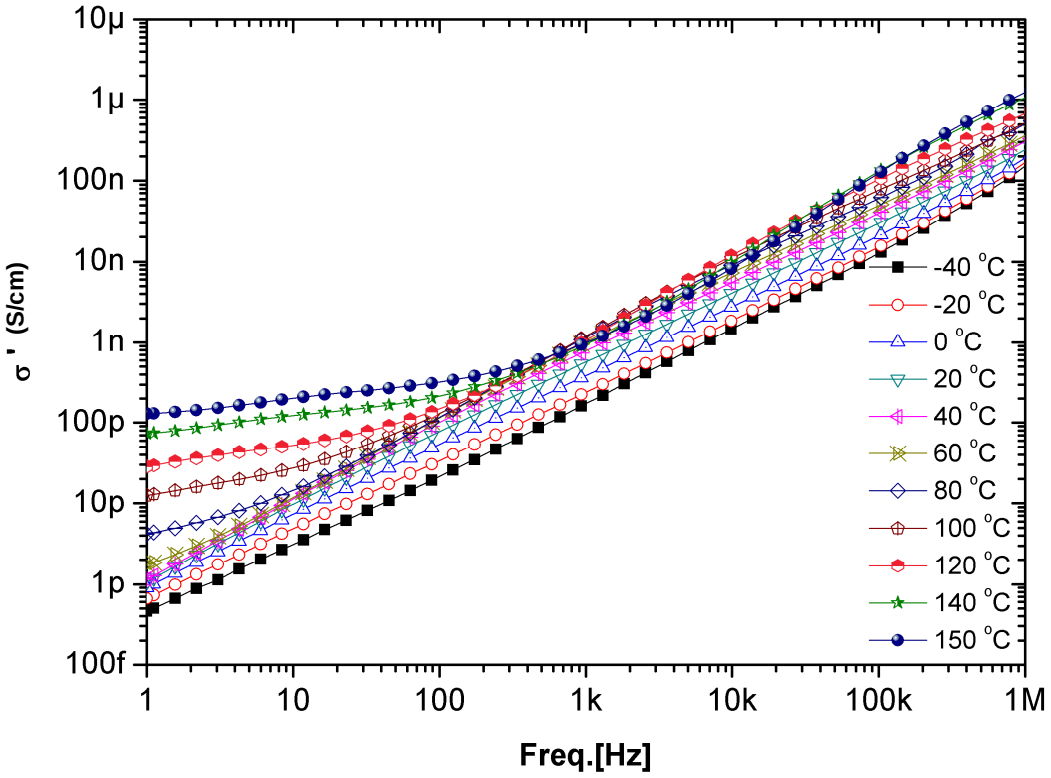

Figure 4.15 The real part of the conductivity of the sample 3E

Figure 4.15 shows σ', the real part of the conductivity value of the sample 3E at varying temperature and frequencies.

It is seen that there is a direct proportionality between the σ' value of the sample and the frequency of the external electric field applied as in all other samples. The conductivity values are between 5.10^{-13} and 10^{-6} S/cm. Here, we again see that the effect of the increasing frequency is extremely predominant on the conductivity values. Moreover, the linearity of the graph is distorted after a certain temperature value like 80^{o}C. For temperatures higher than this value, we observe the distinction of the low frequency and high frequency regions again. At low frequency region, we see the slight frequency dependency whereas at high frequency region the linear relationship is still conserved. The order of the conductivity almost increases at about the order of 3 for 1 Hz spot frequency where the increment is larger than the order of 1 at the larger frequencies between the lowest and the highest temperature. It is easy to see

that 3D graph is quite similar to 3C since the DC conductivity part is more separated and the moderate frequency part is quite much squeezed compared to 3C and 3D.

4.4 The Effect of PMMA Incorporation in Column C Samples

In this part we analyze the affect of polymer ratio on the real part of the dielectric constant and conductivity at 20°C and 120°C and at varying frequency range.

4.4.1 The Real Part of the Dielectric Constant of Column C Samples at 20°C and 120°C

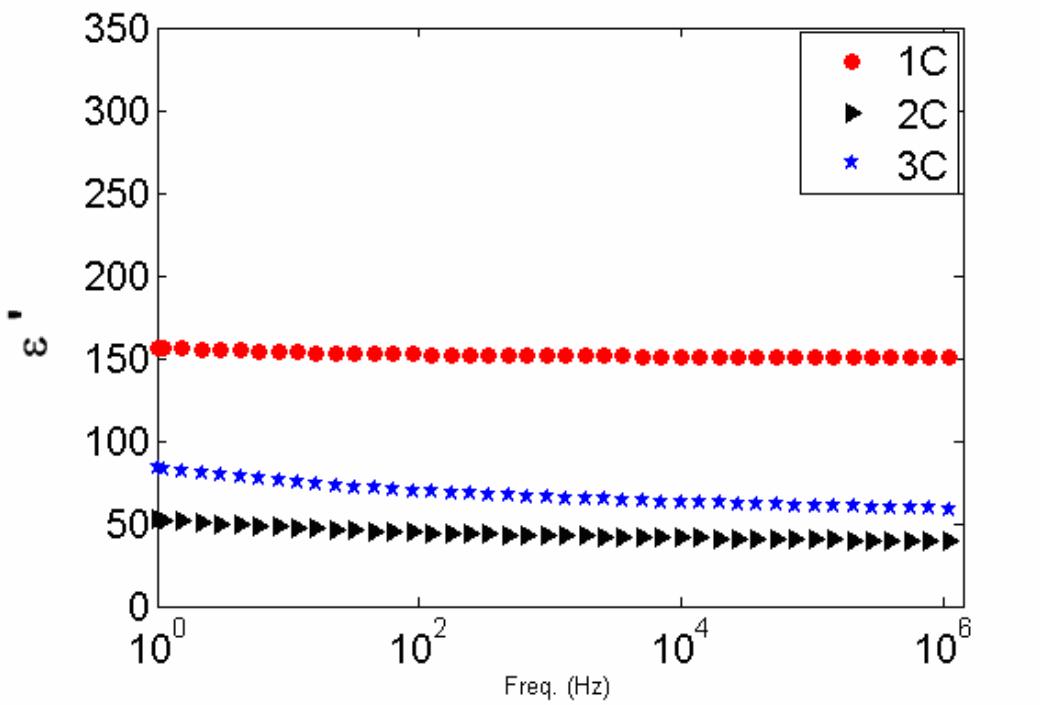

Figure 4.16 The real part of the permittivity of the column C samples at 20°C

Figure 4.16 shows the ε' of the samples 1C, 2C and 3C that have equal amount of cobalt and complex ferrite and decreasing polymer ratio respectively at 20°C under varying frequencies. Note that sample 3C has the 1/3 polymeric ratio of the sample 1C and 2/3 of sample 2C.

We easily notice that ε' values are almost frequency independent for all samples at this temperature. Among the samples the sample with the greatest polymeric ratio,1C has the

maximum values of the real part of the permittivity. Its value is 150 and is almost 3 times larger than the other values.

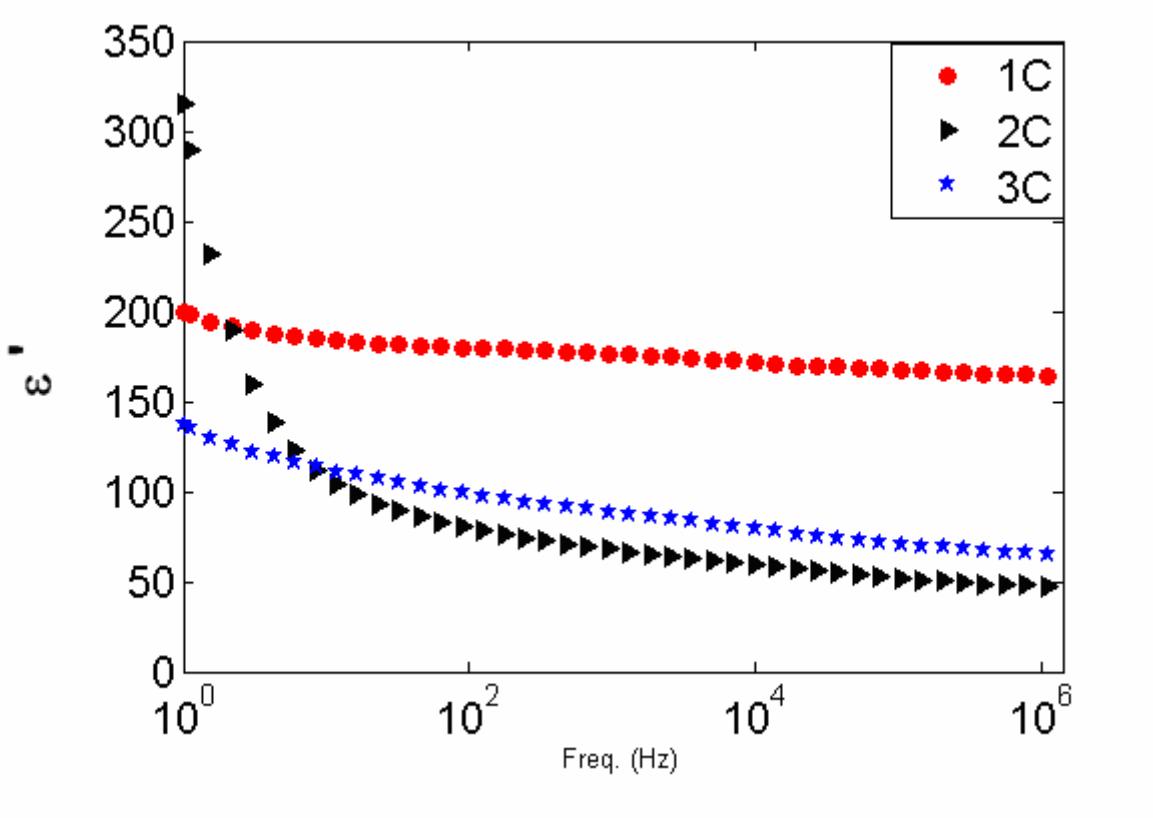

Figure 4.17 The real part of the permittivity of the column C samples at 120^{o}C

Figure 4.17 shows the ε' of the samples 1C, 2C and 3C that have equal amount of cobalt and complex ferrite and decreasing polymer ratio respectively at 120^{o}C under varying frequencies.

Notice that, ε' values are almost frequency dependent for all samples at this temperature. Sample 1C shows the least frequency dependency whereas sample 2C shows the maximum dependency, especially at low frequency region. Sample 2C and sample 3C follow almost the same route after 10 Hz but much before this frequency 2C takes greater values even than 1C which has the highest permittivity values in both low and high temperatures.

4.4.2 The Real Part of the Conductivity of Column C samples at 20°C and 120°C

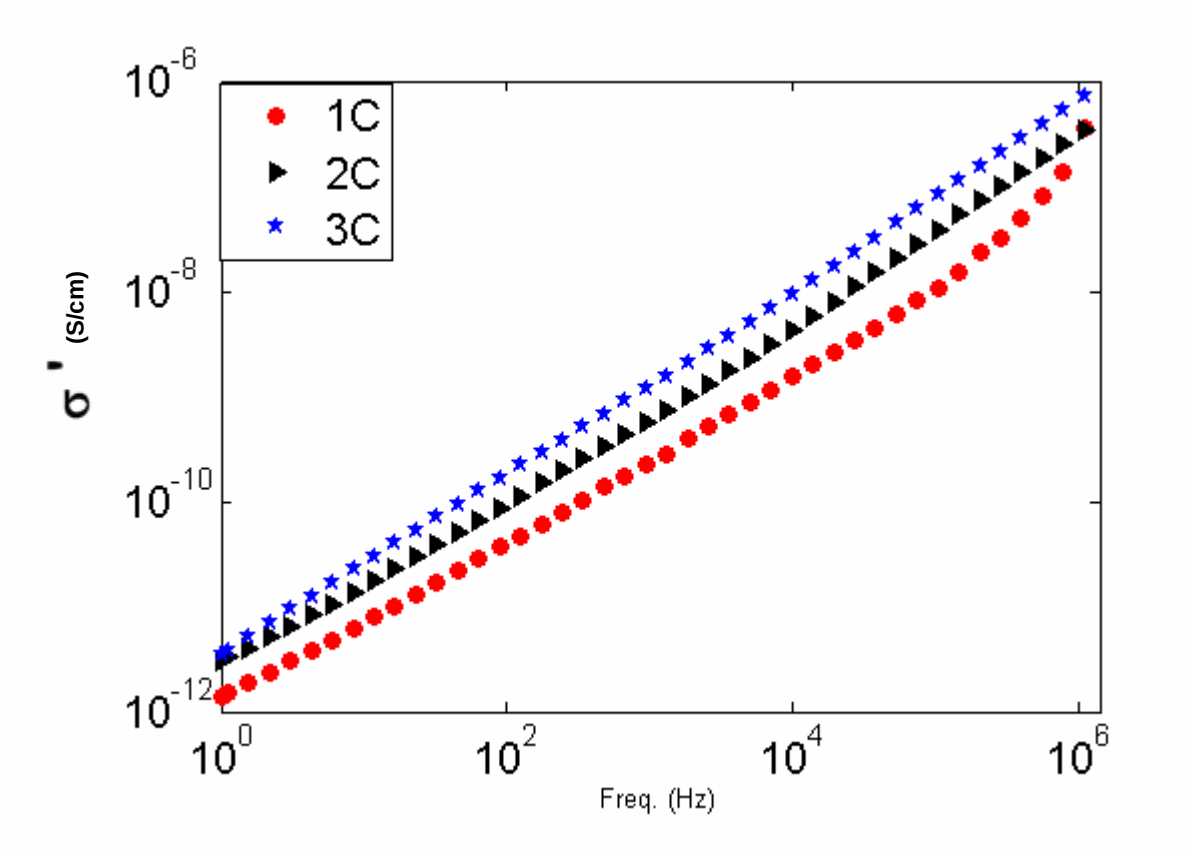

Figure 4.18 The real part of the conductivity of the column C samples at 20°C

Figure 4.18 shows the σ', the real part of the conductivity of the samples 1C, 2C and 3C that have equal amount of cobalt and complex ferrite and decreasing polymer ratio respectively at 20°C under varying frequencies.

First of all, σ' of the all samples increases with frequency and the values are in between 10^{-12} and 10^{-6} S/cm. Notice that, the sample with the least polymer ratio, 3C has the maximum conductivity. So, we can say polymer doping decreases σ' value slightly at this temperature.

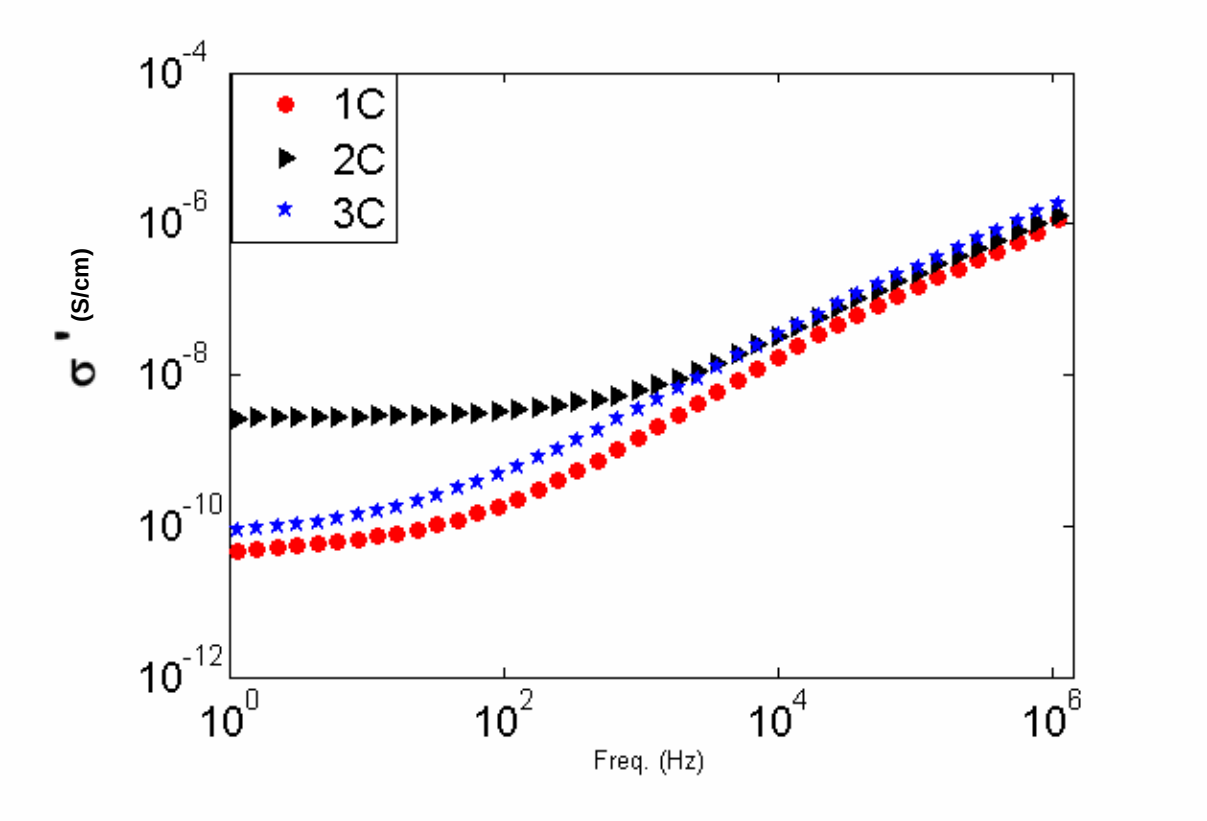

Figure 4.19 The real part of the conductivity of the column C samples at 120°C

Figure 4.19 shows the σ', the real part of the conductivity of the samples 1C, 2C and 3C that have equal amount of cobalt and complex ferrite and decreasing polymer ratio respectively at 120°C under varying frequencies.

At first sight, we can say σ' of the all samples increases with frequency and the values are in between 10^{-10} and 10^{-6} S/cm. However, it can be seen that at frequencies that is smaller than a few 100 Hz, we see a frequency independency, namely DC conductivity but for higher frequency part the linear relationship is still conserved. 2C, sample with the moderate polymer ratio significantly prevails. Its conductivity is almost 100 times greater than the others. We may explain this situation by the well separation of the polymer into the body at its glass transition temperature T_g of 120°C so that it adds to so called semiconductor-type hopping conduction [63].

CHAPTER 5

5. CONCLUSION

5.1 Dielectric Strength Values of Line 3 Samples

Temperature dependent dielectric spectroscopy (DS) is employed for acquiring information about the electrical behaviors of ferrite doped polymer samples of various ratios. The complex dielectric permittivity is given as, $\varepsilon = \varepsilon' - i\varepsilon''$, where ε' is the real part, and ε'' is the imaginary part of the dielectric constant. The real part of the dielectric constant was calculated from the equation, $\varepsilon' = C_p d/(\varepsilon_0 A)$ where C_p is the parallel capacitance, d is the inter-electrodes distance, ε_0 is the permittivity of free space and A is the plate area. Our main fictions in these measurements are focused primarily on the peculiarity of real dielectric constant, ε', of PMMA composite. Figure 5.1 implies the fact that the real part of the dielectric permittivity is decreasing while the frequency is rising. Actually these variations are depending on the ratios of the compositions. In order to account for this variation, one can call the difference between the minimum and maximum values of dielectric constants as dielectric strength (Δε), which can be interpreted as followings;

$$\Delta\varepsilon = \varepsilon_0 - \varepsilon_\infty \tag{5.1}$$

where ε_0 is the dielectric constant at lowest frequency, and ε_∞ is the dielectric constant at highest frequency. Table 5.1 depicts the dielectric strength (Δε) values of these composites.

Table 5.1 Dielectric Strength (Δε) values of the samples at various temperatures

Δε	**-40 °C**	**-20 °C**	**0 °C**	**20 °C**	**40 °C**	**60 °C**	**80 °C**	**100 °C**	**120 °C**	**140 °C**
3A	3.66	4.81	6.18	7.55	8.5	9.12	11.56	17.53	31.39	40.58
3B	5.36	7.77	10.69	13.51	15.82	17.13	17.85	21.87	40.23	47.58
3C	7.36	11.07	17.26	25.02	31.9	35.89	41.31	52.83	73.19	93.75
3D	3.11	4.81	7.17	9.68	11.69	13.56	18.08	27.63	34.8	41.19
3E	2.76	4.38	6.79	9.52	11.97	13.66	16.2	23.36	33.15	44.79

5.2 The Dielectric Peculiarity of the Samples

Firstly, it is noteworthy to distinguish the maximum values of sample 3C. This sample contains complex ferrite and cobalt ferrite at the same ratios and dielectric peculiarity of this sample is simply increasing with the increase in temperature. In order to make comments on relative situation of the other samples merely, cobalt Ferrite and complex ferrite containing 3A and 3E samples were analyzed and it was observed that Δε of sample 3A is more effective at temperatures below 0 ^{o}C while sample 3E is more effective above 0 ^{o}C. Some further optimization is performed by exploiting 3B and 3D along the temperatures until 80 ^{o}C. Actually 3B shows strong and 3D shows weak dielectric strength effect in this interval. The situation is just reciprocal above 80 ^{o}C, namely 3B shows weak and 3D shows strong behavior.

The best dielectric peculiarity is exhibited in 3C and this is valid for all temperatures. Also one should look for the imaginary part of dielectric behavior for the energy dependency of materials. In fact imaginary dielectric constant could be distinguished as the energy loss and here imaginary part of ferrite doped PMMA gives us information about the order of AC conductivity [20].

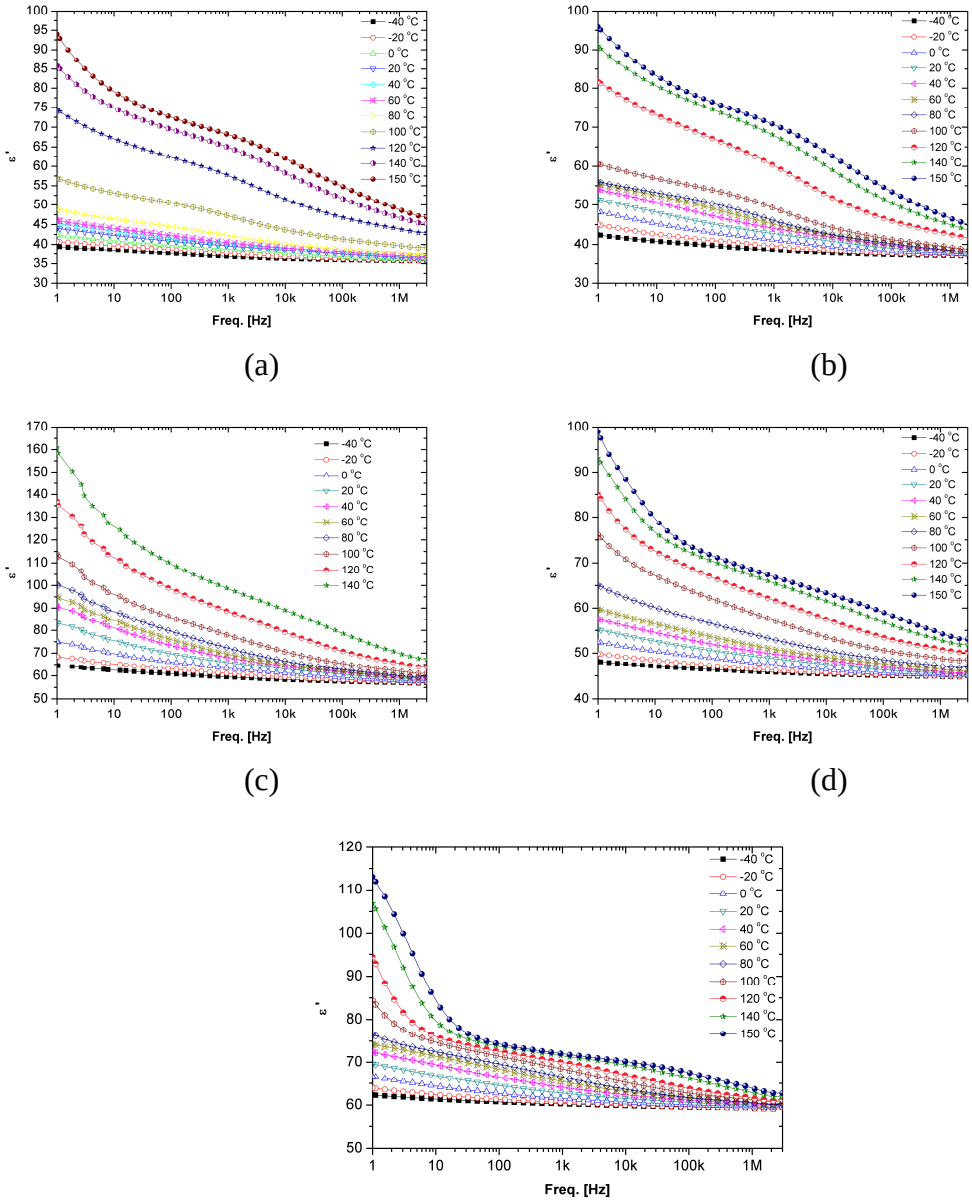

Figure 5.1 Frequency dependency of the real part of dielectric constant at various temperatures for; a) 3A, b) 3B, c) 3C, d) 3D, e) 3E

5.3 The Relaxation Time and the Absorption Coefficient Values

Complex dielectric equation can be written as [60],

$$\varepsilon^{*} = \varepsilon_{\infty} + \frac{(\varepsilon_0 - \varepsilon_{\infty})}{1 + (i\omega\tau)^{1-\alpha}} \tag{5.2}$$

where ε_o is the low frequency dielectric value and ε_{∞} is the high frequency dielectric value in the measured frequency interval, ω is the angular frequency, τ is the relaxation time and α is the absorption coefficient. Debye equation can be inspired from Eq. 5.2 for the merely real dielectric portions and it can be written as [63].

$$\varepsilon'(\omega) = \varepsilon_{\infty} + (\varepsilon_s - \varepsilon_{\infty}) \frac{1 + (\omega\tau_0)^{1-\alpha} \sin\frac{1}{2}\alpha\pi}{1 + 2(\omega\tau_0)^{1-\alpha} \sin\frac{1}{2}\alpha\pi + (\omega\tau_0)^{2(1-\alpha)}} \tag{5.3}$$

These measured values of real dielectric constant are fitted to above function for different temperatures (-40 ^{o}C, 20 ^{o}C, 80 ^{o}C, 140 ^{o}C) and relaxation time τ and the absorption coefficient α were acquired from this fit and these values are given in Table 5.2. These values contain information about Debye type characteristics of the samples. Absorption coefficient values are between $0 \leq \alpha \leq 1$ and if it is 0 then Debye type behavior is dominant if it is nonzero then non-Debye behavior is dominant [64]. It is obvious from α values that all ferrite samples demonstrate non-Debye character and their values are between 0.5 and 0.7.

Table 5.2 The absorption coefficient α and the relaxation time, τ values for all samples

α	**-40^{0}C**	**20^{0}C**	**80 ^{0}C**	**140^{0}C**
3A	0.58252	0.69516	0.66238	0.70143
3B	0.56159	0.61779	0.61243	0.6748
3C	0.60027	0.64698	0.63112	0.70037
3D	0.56251	0.66468	0.63544	0.70324
3E	0.68591	0.58286	0.63737	0.65048
τ (s)				
3A	0.02421	0.00149	0.002	0.00186
3B	0.00633	0.00421	0.00155	0.00117
3C	0.00457	0.00817	0.00694	0.01015
3D	0.01275	0.00337	0.00567	0.01037
3E	0.00163	0.00656	0.00279	0.07475

3B exhibits the fastest relaxation time value among the samples for all temperatures. Also the relaxation time τ is decreasing with temperature rise for 3B and this is simply an indicator of short term dipole-dipole interactions, namely higher conductivity values with the mentioned temperature rise. This kind of temperature dependency is actually revealing the semi-conducting behavior caused by ferrite concentration [64]. Fig. 5.2 confirms this argument explicitly, and 140 ^{o}C is the best response temperature for PMMA with Cobalt Ferrite.

5.4 The Real part of the Conductivity Values of the Samples

The real part of conductivity σ' is in consistency with the imaginer permittivity values according to, $\sigma^{'} = \omega\varepsilon^{''}\varepsilon_o$ here ω is the angular frequency. Fig. 5.2 demonstrates the variations of AC conductivity as a function of frequency at different temperatures.

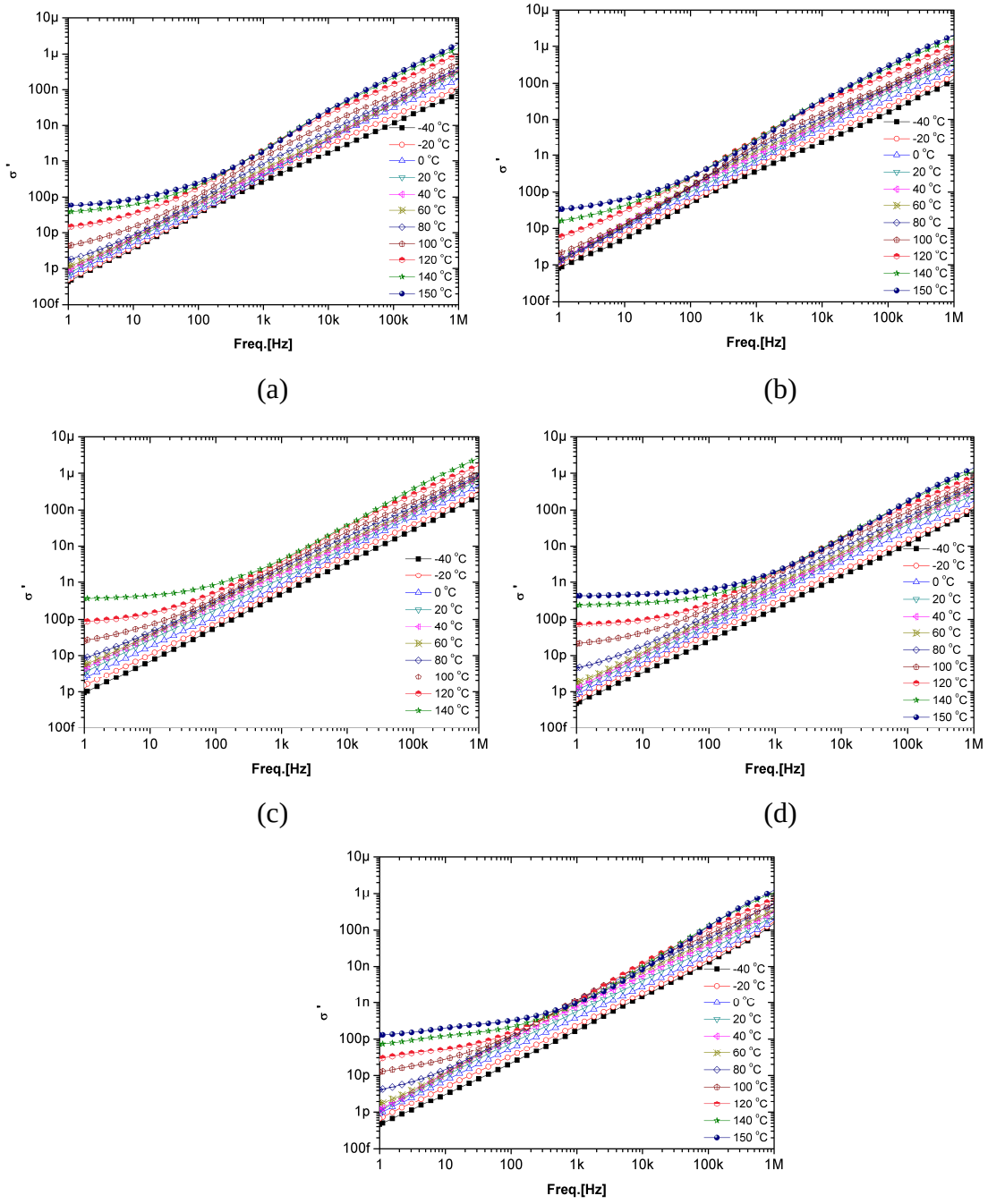

Figure 5.2 The variations of conductivity as a function of frequency at different temperatures for samples; a) 3A, b) 3B, c) 3C, d) 3D, e) 3E

Weak temperature dependency of conductivity at high frequencies and strong temperature dependency at low frequencies are caused by semi-conducting properties of the ferrite. Furthermore, Fig. 5.2 shows AC conductivity depends on the frequency plots in the

temperature range of -40^{0}C to 140^{0}C with 20 ^{o}C ramps. As it can be seen from this analysis, the increase in the ratio of complex ferrite to cobalt ferrite causes stronger temperature dependency at higher temperatures, again verifying the dominancy of the semi-conductor property.

5.5 Activation Energies of the Samples

Fig. 5.3 shows AC conductivity plots of ln(σ) versus 1000/Temperature (K^{-1}) and it was calculated by the equation $\sigma = \sigma_0 \exp(-E/(kT))$ for the concerned samples at 1 Hz spot frequency. It is clear from the figure that the conductivity exhibits a ferritic-semiconductor behavior along the temperature rise. Here we have investigated the panorama in two main regions exhibiting different tendency. One can call these regions as high temperature and low temperature regions according to activation energies whose values are determined from the so called Arrhenius law:

$$\sigma = \sigma_o \left[\exp(-E_I/(kT)) + \exp(-E_{II}/(kT))\right] \qquad (5.4)$$

Here σ_o is conductivity constant, E_I and E_{II} are the activation energies in the Region I and Region II, respectively and *k* is the Boltzmann constant.

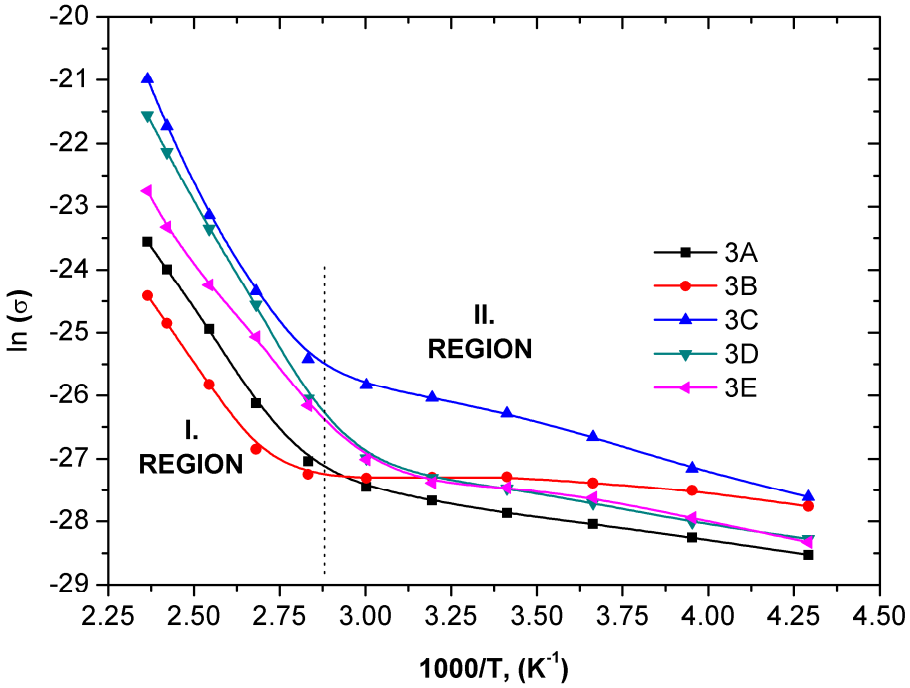

Figure 5.3 Arrhenius plots of conductivity for 3A, 3B, 3C, 3D, 3E coded samples at 1 Hz spot frequency.

The calculated activation energies of these two regions were depicted in Table 5.3. In fact, activation energy is a function of temperature, and it gives information about the required energy for keeping the material altogether in the matrix structure. In addition, we tried to acquire information about the trend of the change of Activation Energy at high and low temperatures at low frequencies, which is the critical region in polymers [40]. Activation Energy is more effective at high temperature region. Again the sample 3B is dominant according to activation energy. This situation is also caused by the Cobalt Ferrites. As it was mentioned before, Cobalt Ferrite is more anisotropic and exhibits a better conductivity while the Complex Ferrite shows cohesive behavior in the prepared matrixes. If we compare the activation energy of 3B in high and low temperature regions it is obvious that so called activation energy is higher at high temperatures so the polymer matrix is more accommodating at higher temperatures for the previously optimized 3B sample.

Table 5.3 Activation energy dependency at the 1 Hz spot frequency

Ea (eV)	**1 [Hz]**	
	E_I	E_{II}
3A	0.84216	0.06988
3B	0.87693	0.02985
3C	0.77585	0.12179
3D	0.78628	0.08363
3E	0.80615	0.08093

As a result, these samples exhibit significant dielectric behaviors at certain frequency and temperature ranges. The different compositions of cobalt and complex ferrites in polymeric matrixes may have excellent challenges in many application areas such as microwave absorbing devices, nanobiosensors etc.

In conclusion, the synthesis of new material composites and their analysis have a very important role in designing new technological advances for human being.

REFERENCES

[1] K. Jia, T.E. Fischer, B. Gallois, Nanostructured Materials. Vol. 10. No. 5. pp. 815491.1998

[2] http://www.engr.utexas.edu/che/nano/

[3] H. Kavas, A. Baykal, M. S. Toprak, Y. Köseoglu, Murat Sertkol, Bekir Aktas J. All. Comp. 479 (2009) 49–55

[4] Huiching Chang. Magnetic Properties and Structure of Pulsed Laser Deposited Nickel Ferrite Films, 2008

[5] http://wikis.lib.ncsu.edu/index.php/Spinel

[6] Victoria L. Calero Díaz Del Castillo Synthesis and Characterization of Cobalt-Substituted Ferrite Nanoparticles Using Reverse Micelles, 2005

[7] I.H. Gul, W. Ahmed, A. Maqsood, J. Magn. Magn. Mater. 320 (2008) 270–275

[8] Muhammad Javed Iqbal, Mah Rukh Siddiquah J. Magn. Magn. Mater. 320 (2008) 845–850

[9] http://wikis.lib.ncsu.edu/index.php/Image:Size21.png

[10] A. Baykal, N. Kasapoğlu, Z. Durmuş, H. Kavas, M. S. Toprak, Y. Koseoğlu, Turk J Chem 33 (2009), 33 – 45.

[11] A. Goldman, *Modern Ferrite Technology*. New York: Van Nostrand Reinhold,

[12] V. Pillai, D. O. Shah, J. Magn. Magn. Mater.163 (1996) 243-248,.

[13] Ovidiu Caltuna,_, Ioan Dumitrua, Marcel Federb, Nicoleta Lupuc, Horia Chiriacc Journal of Magnetism and Magnetic Materials 320 (2008) e869–e873

[14] I.H. Gul, A. Maqsood, J. Alloys & Comp. 465 (2008) 227–231

[15] Xiangchun Liua, Feng Gaob, Jiaji Liub, Changsheng Tianb, J. All. Comp. 470 (2009) 269–272

[16] Jiang Li Cao, Xiao Hui Wang, Li Zhang, Long Tu Li Materials Letters 57 (2002) 386–391

[17] http://en.wikipedia.org/wiki/Acrylic_glass

[18] A. K. Adiyodi, X. Joseph, P. V. Jyothy, G. Jose, N. V. Unnikrishnan *Materials Science-Poland, Vol. 27, No. 1, 2009*

[19] http://en.wikipedia.org/wiki/File:PMMA_acrylic_glass.png

[20] F. Gözüak, Y. Köseoğlu, A. Baykal, H. Kavas J. Magn. Magn. Mater. 321 (2009) 2170-2177.

[21] M. Sertkol, Y. Köseoğlu, A. Baykal, H. Kavas, A. C. Başaran, J. Magn. Magn. Mater. 321 (2009) 157.

[22] Y. Köseoğlu, H. Kavas, J. Nanosci. and Nanotech. 8 (2008) 584.

[23] Y. Köseoğlu, H. Kavas, B. Aktaş, Phys. Stat. Sol. (a) 203 (2006) 1595.

[24] http://www.international.inra.fr/partnerships/with_the_private_sector/live_from_the_labs/nanobiosensors_the_most_recent_nanotechnological_noses

[25] Nai Sheng Chen, Xiao Juan Yang, Er Sheng Liu, Jin Ling Huang Sensors and Actuators B 66_2000.178–180

[26] E. Rezlescu, N. Iftimie, P. D. Popa and N. Rezlescu Journal of Physics: Conference Series 15 (2005) 51–54

[27] Giovanni Baldia, Daniele Bonacchia, Claudia Innocentib, Giada Lorenzia, Claudio Sangregoriob, J. Magn. Magn. Mater. 311 (2007) 10–16

[28] http://arstechnica.com/science/news/2008/07/extracting-cancer-cells-with-magnetic-nanoparticles.ars

[29] www.rsc.org/Publishing/Journals/cb/Volume/2008/1/turning_up_the_heat_on_cancer.asp

[30] Winfried Mollera, Shinji Takenakaa, Norbert Buskeb, Kathrin Feltena, Joachim Heyder J. Magn. Magn. Mater. 293 (2005) 245–251

[31] JianLiang Xiea, Mangui Hana, Liang Chena, Renxiong Kuanga, Longjiang Denga, J. Magn. Magn. Mater. 314 (2007) 37–42

[32] Y. Nie, H. He, Z. Zhao, R. Gong, H. Yu, J. Magn. Magn. Mater.
306 (2006) 125.

[33] T. Kasagi, T. Tsutaoka, K. Hatakeyama, Appl. Phys. Lett. 88 (2006) 172502.

[34] M. Han, L. Deng, Appl. Phys. Lett. 90 (2007) 0111081.

[35] P. Lubitz, F.J. Rachford, J. Appl. Phys. 91 (2002) 7613.

[36] Z.W. Li, L. Chen, C.K. Ong, J. Appl. Phys. 94 (2003) 5918

[37] S.M. Abbasa, A.K. Dixit, R. Chatterjeea, T.C. Goelc, J. Magn. Magn. Mater. 309 (2007) 20–24

[38] A.N. Yusoff, M.H. Abdullah, J.Magn. Magn. Mater. 269 (2004) 271.

[39] C.H. Peng, C.C. Hwang, J. Wan, J.S. Tsai, S.Y. Chem, Mater. Sci. Eng. B 117 (2005) 27.

[40] D.K. Kim, M. Toprak, M. Mikhaylova, Y. S. Jo, Steven J. Savage, T. Tsakalakos, M. Muhammed, Solid State Phenomena, 99-100, 165-168, 2004.

[41] http://en.wikipedia.org/wiki/File:F-117_Nighthawk_Front.jpg

[42] K. C. Kao, Dielectric Phenomena in Solids, 2004

[43] R.H. Cole, “Theories of Dielectric Polarization and Relaxation”, in *Progress in Dielectrics*, Vol. 3, (Heywood, London, 1961) pp. 47–100.

[44] http://mendonphysics2007p9.blogspot.com/2008/03/leyden-jar.html

[45] A.K. Jonscher, *Dielectric Relaxation in Solids*, (Chelsea Dielectric Press, London, 1983).

[46] http://www.school-for-champions.com/chemistry/polar_molecules.htm

[47] J.H. van Vleck, *Theory of Electric and Magnetic Polarizabilities*, (Oxford Univeristy Press, Oxford, 1932).

[48] J. Ravez, C. R. Acad. Sci. Paris, Serie IIc, Chimie : Chemistry 3 (2000) 267–283

[49] http://en.wikipedia.org/wiki/Ferroelectricity

[50] C.P. Smyth, *Dielectric Behavior and Structure*, (McGraw-Hill, New York, 1955).

[51] http://www.doitpoms.ac.uk/tlplib/dielectrics/polarisation_mechanisms.php

[52] http://www.tf.uni-kiel.de/matwis/amat/elmat_en/kap_3/backbone/r3_2_4.html

[53] http://aph.huji.ac.il/courses/2008_9/83887/index.html

[54] L.D. Landau, E.M. Lifshitz Electrodynamics of Continuous Media, 1984

[55] C.J.F. Boetcher Theory of Electric Polarization 2D ED. 2 volumes 1973-1978.

[56] M. Born and K. Huang, *Dynamical Theory of Crystal Lattices*, Oxford, 1954).

[57] N.E. Hill, W.E. Vaughan, A.H. Price, and M. Davies (Eds.), *Dielectric Properties and Molecular Behaviour*, (Van Nostrand Reinhold, London, 1969).

[58] C.H. L. Goodman, Physics of Dielectrics Solids, 1980

[59] P.Q. Mantas, “Dielectric Response of Materials: Extension to the Debye Model”, J. The European Ceramic Society 19 (1999) 2079-2086.

[60] Huang C, Zhang Q 2004 Adv. Funct. Mater. 14 501.

[61] A.Qureshi, A. Mergen, Bekir Aktas, doi:10.1088/1742-6596/153/1/012061

[62] W.Shi, C. Fang, Q. Pan, X.Sun, Q. Gu, D. Xu, J. Yu, Reactive & Functional Polymers 44 (2000) 177–182)

[63] G.G. Raju, Dielectrics in Electric Fields (Marcel Dekker, 2003)

[64] E. Sentürk, M. Okutan, S.E. San, O. Köysal Journal of Non-Crystalline Solids 354 (2008) 3525–3528.